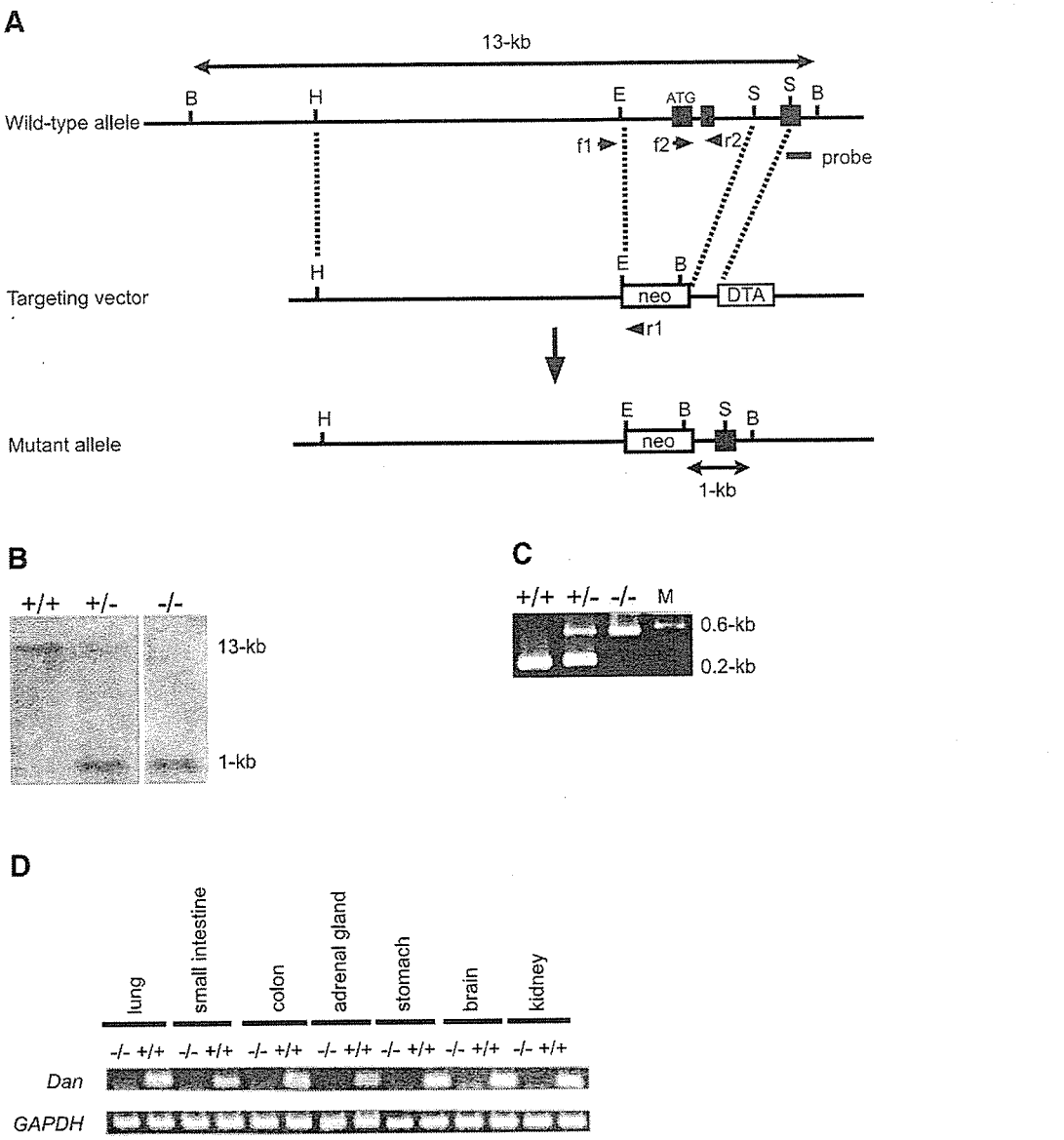

Fig. 1. Generation of Dan-deficient mice. (A) Schematic drawing of gene targeting strategy. The map of the wild-type *Dan* allele spans the region between intron I and exon IV (top). Filled boxes indicate the exons II, III, and IV. The targeting vector (middle) was constructed as described in the Experimental methods. Arrowheads indicate the locations of PCR primers used for detecting the wild-type or mutant allele: forward-1 (f1) and reverse-1 (r1) for the mutant allele, and forward-2 (f2) and reverse-2 (r2) for the wild-type allele. The location of the probe (0.4-kb *Sma*I–*Xba*I restriction fragment) used for Southern analysis is indicated by the solid bar. This probe detects 13- and 1-kb fragments derived from the wild-type and the mutant alleles, respectively. The mutant allele is shown below the targeting vector. B, *Bam*HI; H, *Hin*cII; E, *Eco*RI; S, *Sma*I. (B) Southern blot analysis of tail DNA from wild-type (+/+), heterozygous (+/−), and homozygous (−/−) mutant mice. Genomic DNA was digested with *Bam*HI, transferred to a nylon membrane, and hybridized with the external probe shown in A. The positions of migration of the fragments derived from wild-type (13 kb) and disrupted alleles (1 kb) are indicated. (C) PCR analysis of tail DNA from wild-type (+/+), heterozygous (+/−), and homozygous (−/−) mutant mice. PCR products were separated on a 2% agarose gel by electrophoresis and visualized by ethidium bromide staining. The positions of migration of the fragments derived from wild-type (0.2 kb) and disrupted alleles (0.6 kb) are indicated. M, DNA molecular weight marker. (D) RT-PCR analysis of *Dan* expression in wild-type (+/+) and homozygous (−/−) mutant mice. Total RNA was prepared from the indicated adult mouse organs and subjected to RT-PCR using specific primers for *Dan* or *GAPDH*. Amplification of *GAPDH* was used as an internal control.

SP, CGRP, NK1, and Dan in the primary sensory neurons under physiological conditions

Double-staining for Dan with CGRP, IB4, P2X3, or NF200

SP- and CGRP-IR neurons were observed in the DRG of both wild-type and Dan-deficient mice (Fig. 2). These neurons were small to intermediate in size. We found that 69 ± 7% (mean ± SE) of all DRG neurons were Dan-IR in wild-type mice, whereas none of DRG neurons were Dan-IR in Dan-deficient mice ($P < 0.01$). The distributions and percentages of SP- and CGRP-IR DRG neurons were not significantly different between wild-type and Dan-deficient mice (wild-type, SP: 26 ± 4%, CGRP, 38 ± 6%;

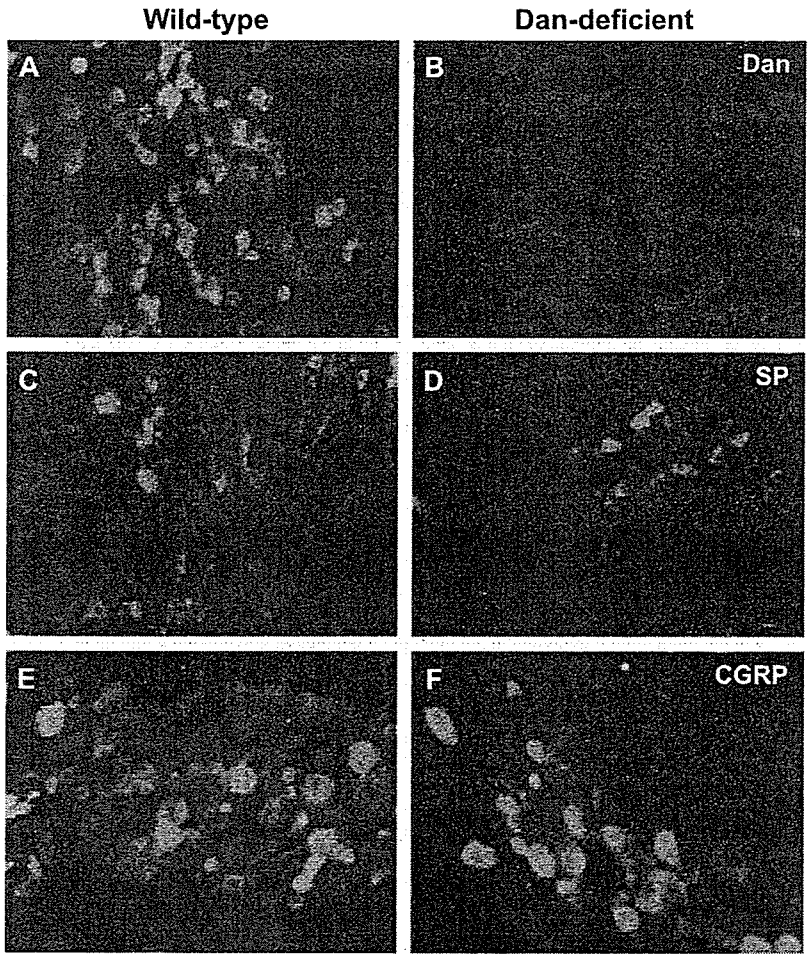

Fig. 2. Dan was absent in DRG neurons of Dan-deficient mice (B). DRG neurons derived from wild-type (A, C, and E) and Dan-deficient mice (B, D, and F) were reacted with antibody to Dan (A and B), substance P (SP) (C and D), or calcitonin gene-related peptide (CGRP) (E and F).

Dan-deficient, SP: 23 ± 5%; CGRP, 42 ± 7%) (mean ± SE) ($P > 0.1$). In the spinal dorsal horn of wild-type mice, Dan-IR sensory nerve terminals were observed in the inner part of lamina II, and SP- and CGRP-IR sensory nerve terminals were observed in laminae I and II (Fig. 3). NK1-IR neurons were detected mainly in laminae I and III. The patterns of SP-, CGRP-, and NK1-IR terminals in the spinal dorsal horn were not significantly different between wild-type and Dan-deficient mice.

Dan-IR nerve fibers were observed where a dorsal root lesion was made in wild-type mice (Fig. 3). Dan-IR free nerve endings were observed in the dermis of the footpads of wild-type mice, but not detectable in the skin of the footpads of Dan-deficient mice (Fig. 3). Two weeks after spinal nerve root section, the number of Dan-IR nerve terminals in the spinal dorsal horn decreased in wild-type mice. Because *Dan* mRNA was expressed in small DRG neurons (Ohtori et al., 2002), Dan was produced in small DRG neurons and seemed to be transported into the spinal dorsal horn and skin of footpads.

Dan immunoreactivity was seen in CGRP-, IB4-, and P2X3-IR neurons (Fig. 4). In all of the Dan-IR neurons, the ratios of Dan-IR neurons labeled with CGRP, IB4, or P2X3 were 33 ± 3%, 55 ± 9%, or 64 ± 8% (mean ± SE), respectively. On the other hand, some Dan was co-localized with NF200-IR myelinated A-fiber neurons (12 ± 3%). The ratios of Dan-IR neurons also labeled with CGRP, IB4, or P2X3 were significantly higher than that of neurons labeled with NF-200-IR ($P < 0.01$). Most of the double-labeled neurons were small-sized A-fiber neurons (Fig. 4).

Interestingly, Dan-IR nerve terminals in the spinal dorsal horn were located only in the inner part of lamina II. Interneurons in the inner part of lamina II differ considerably from those located dorsally in lamina I and in the outer part of lamina II. Immunocytochemical studies of the localization of the P2X3 receptor indicated its presence in a subpopulation of small-diameter non-peptidergic neurons that specifically bind IB4; these neurons project to (the inner part of) lamina II in the dorsal horn (Bradbury et al., 1998; Llewellyn-Smith and Burnstock, 1998). Dan-positive small DRG neurons stained with IB4 and P2X3 could project into the inner part of lamina II.

Almost all of the small DRG neurons were Dan-IR. In comparison, it has been reported that, respectively, only 20% and about 40% of small DRG neurons are substance P- and CGRP-containing (Neumann et al., 1996). In the current study, CGRP-IR DRG neurons were double-labeled with Dan. Non-IB4 and P2X3-IR Dan-positive DRG neurons were SP- or CGRP-containing small neurons projecting into lamina I and the outer layer of lamina II. However, it is unclear why Dan immunoreactivity in the spinal

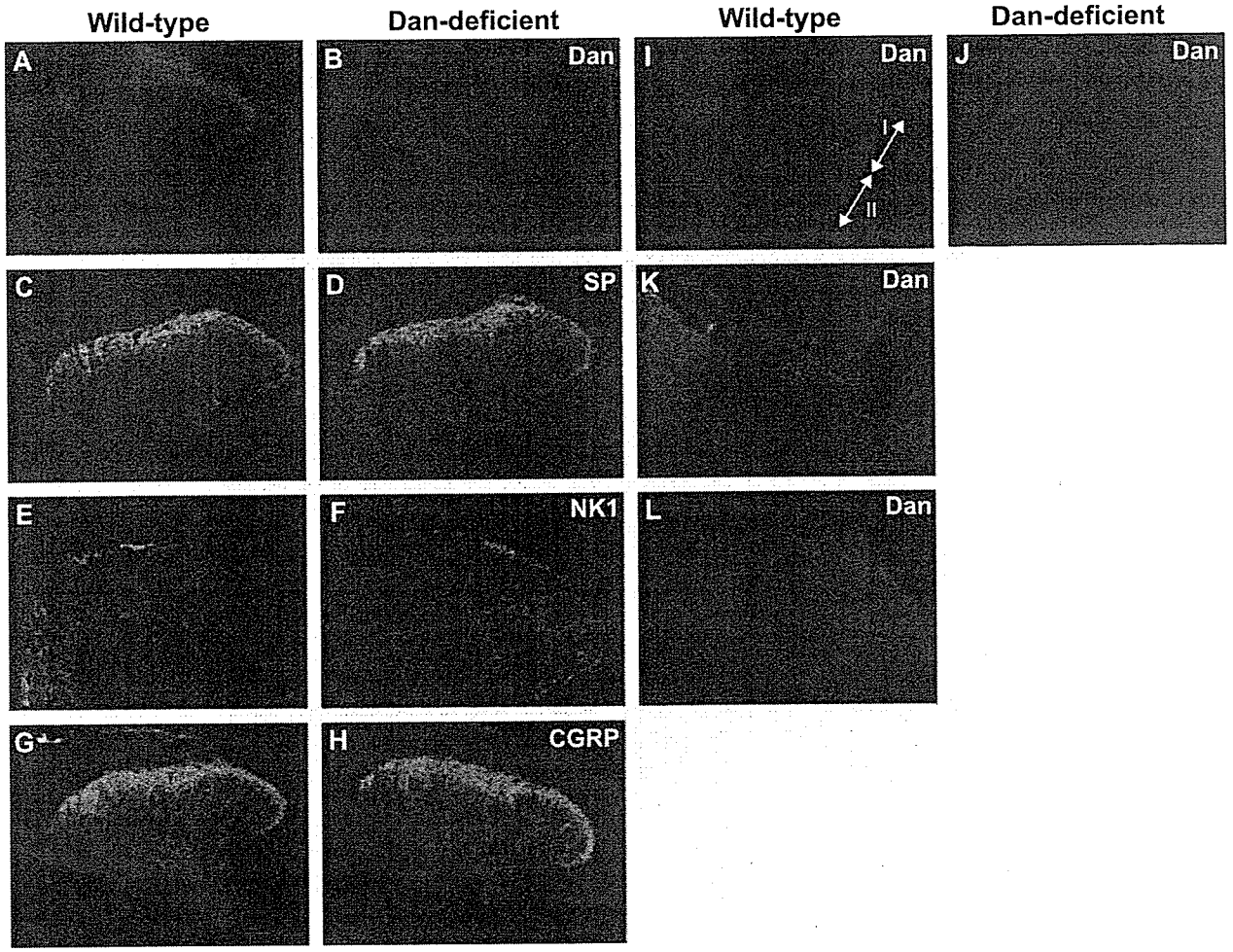

Fig. 3. In wild-type mice, DAN-IR sensory nerve terminals were observed in the inner part of lamina II, whereas Dan was absent in the spinal dorsal horn of Dan-deficient mice (B). In both types of mice, SP- (C and D) and CGRP-IR (G and H) sensory nerve terminals were detected in laminae I and II. Neurokinin receptor (NK1)-IR neurons were observed mainly in laminae I and III (E and F). Dan-IR sensory nerve endings in the dermis of footpads and sensory nerves in spinal dorsal root lesion were seen in wild-type mice (I and K), whereas they were not observed in the footpads of Dan-deficient mice (J). I, Epidermis; II, Dermis. Dan-IR nerve terminals in spinal dorsal horn decreased 2 weeks after dorsal root cut (L).

dorsal horn is seen only in the inner part of lamina II. One possible reason is that Dan protein in peptidergic neurons may not be transported to the central terminals in the spinal cord.

It has been reported that specific TGF-β family members are candidate regulators of CGRP expression in embryonic sensory neurons. BMPs 2, 4, and 6 stimulated CGRP expression in 60% of DRG neurons. BMP4 application supported maximal CGRP induction, suggesting that BMP4 is a "switch" rather than a continuous modulator of neuropeptide phenotype (Ai et al., 1999). In our study, we did not observe any differences in the distributions and ratios of SP- and CGRP-IR DRG neurons and sensory terminals in the spinal dorsal horn under physiological conditions. Dan seems not to regulate CGRP expression in embryonic and adult sensory neurons.

Thermal hypersensitivity and mechanical allodynia after inflammation

In the absence of inflammation or nerve injury, we found no differences in paw withdrawal responses to thermal and mechanical stimulation between Dan-deficient and wild-type mice. In wild-type and Dan-deficient mice, CFA injection produced a significant reduction in paw withdrawal latency to a heat stimulus on the injected side ($P < 0.01$) (Fig. 5A). Also, both types of mice displayed a significant mechanical allodynia ($P < 0.01$) (Fig. 5B). However, this decrease in the threshold of thermal and mechanical allodynia in Dan-deficient mice was significantly less than that of wild-type mice ($^*P < 0.05$). Injury to the sciatic nerve produced a significant decrease in the paw withdrawal threshold to thermal and von Frey hair stimulation on the injured side of wild-type ($P < 0.01$) and Dan-deficient mice ($P < 0.01$); however, the decrease in threshold between the two groups was not significantly different ($P > 0.1$) (Figs. 5C and D).

We previously showed that the Dan protein in rat DRG neurons increased only following CFA injection, but did not change following partial nerve injury. Furthermore, intrathecal injection of an antibody to Dan suppressed only inflammatory pain caused by the introduction of CFA and it did not suppress pain due to nerve injury (Ohtori et al., 2002).

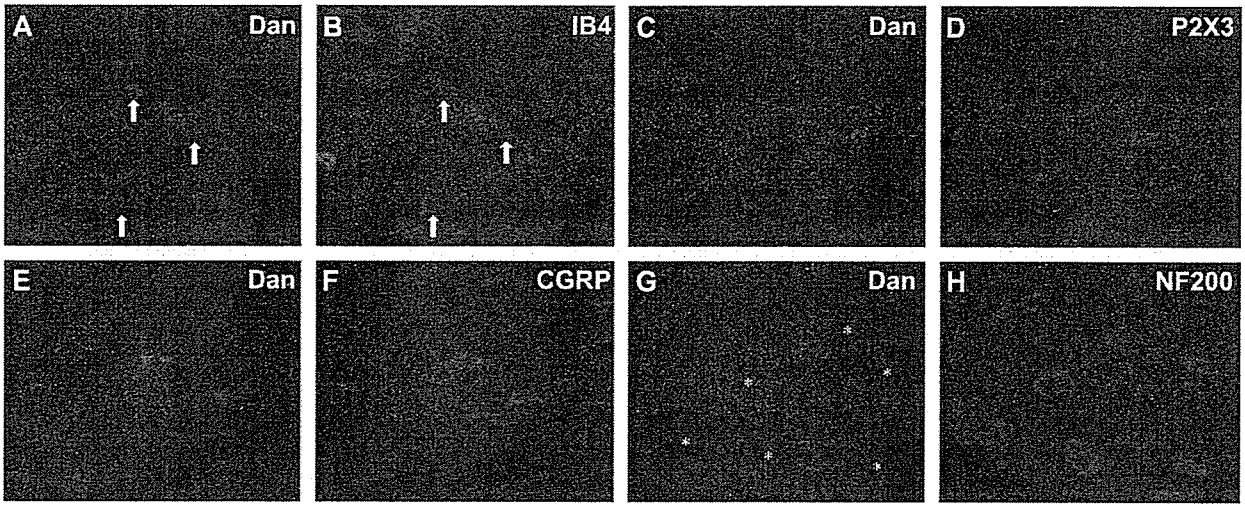

Fig. 4. Micrographs showing double-staining for Dan with isolectin B4 (IB4) (A and B), P2X3 (C and D), CGRP (E and F), or neurofilament 200 (NF200) (G and H). Dan was double-labeled with CGRP-IR DRG neurons. Dan immunoreactivity was seen in most IB4 and P2X3-IR neurons. On the other hand, most of Dan was not double-labeled in NF200-IR myelinated A-fiber neurons. Asterisks indicate Dan-IR and NF200-negative neurons.

It has also been reported that, in inflammatory models, SP and CGRP were increased in the dorsal root ganglia and the dorsal horn of the lumbar spinal cord (Donnerer et al., 1992; Noguchi and Ruda, 1992; Noguchi et al., 1988) and that the neurokinin receptor (NK1) was increased in the dorsal horn (Abbadie et al., 1996; McCarson and Krause, 1994).

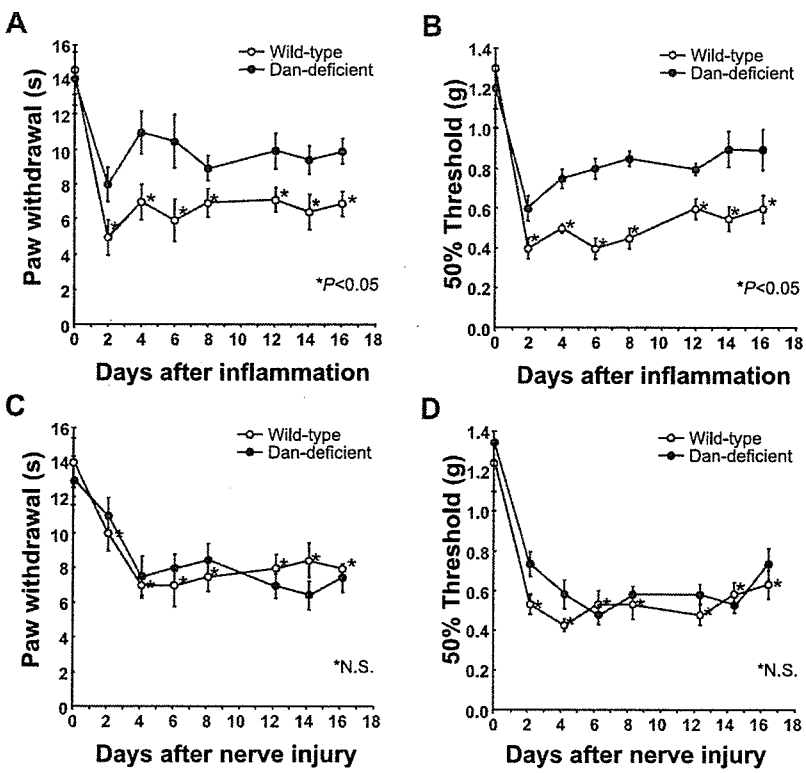

Fig. 5. Hyperalgesia measured by withdrawal to noxious thermal stimulation of the hind paw (A). The data are expressed as the difference in paw withdrawal latency between wild-type and Dan-deficient mice. After injection of CFA, significant reduction in paw withdrawal latency was observed in both types of mice; however, the decrease was significantly different between wild-type and Dan-deficient mice ($P < 0.05$). Inflammation also produced a significant decrease in paw withdrawal threshold (B). Asterisks indicate a significantly lower threshold on the inflammatory side in the wild-type mice compared with that of Dan-deficient mice ($P < 0.05$). Nerve injury also produced hyperalgesia measured by withdrawal to noxious thermal stimulation of the hind paw (C) and a significant decrease in the paw withdrawal threshold to von Frey filament stimulation (D). However, there were no differences between wild-type and Dan-deficient mice ($P > 0.1$).

Indeed, 4 days after inflammation in the current study, the fractions of SP- and CGRP-IR DRG neurons were 40 ± 4% (mean ± SE) and 52 ± 5%, respectively, in wild type and corresponding values for Dan-deficient mice were 31 ± 4% and 49 ± 5% (Figs. 6 and 7). The ratio of SP- and CGRP-IR neurons in both types of mice significantly increased compared with a non-inflammatory control ($P < 0.05$). The ratio of SP-IR neurons in wild-type mice was higher than that in Dan-deficient mice ($P < 0.05$) (Figs. 6 and 7); however, there was no significant difference in the ratio of CGRP-IR neurons in both types of mice after inflammation ($P > 0.1$). The relationship between Dan and other peptides influenced by neuropathic or inflammatory pain remains unclear. It is possible that Dan might induce SP in DRG neurons under inflammatory conditions.

Protein kinase C gamma (PKC) staining is also confined to interneurons of the inner part of lamina II. Mice that lack PKC displayed normal responses to acute pain stimuli, but they almost completely failed to develop a neuropathic pain syndrome after partial sciatic nerve section (Malmberg et al., 1997). On the other hand, the P2X3 receptor is important during inflammatory periods and may play a role in the modulation of spinal nociceptive transmission following the development of inflammation, but these receptors play at most a minor role in spinal nociceptive processing in normal and neuropathic animals (Liu and Tracey, 2000; Stanfa et al., 2000). Dan, which was expressed in the inner part of lamina II, seems to regulate only inflammatory pain.

Depression of Fos expression in inflammatory pain

Fos-IR neurons were present mainly in the left dorsal horn (Figs. 8 and 9). The time course of Fos expression following CFA injection in wild-type and Dan-deficient mice is shown in Fig. 10. The numbers of Fos-IR neurons following CFA injection in the superficial and deep laminae of Dan-deficient mice were significantly less than those in wild-type mice ($P < 0.05$) (Fig. 11A). The amount of Fos expression in lamina II of Dan-deficient mice was significantly less than that in wild-type mice ($P < 0.05$) (Fig. 11C). The difference was detected for all the periods we observed

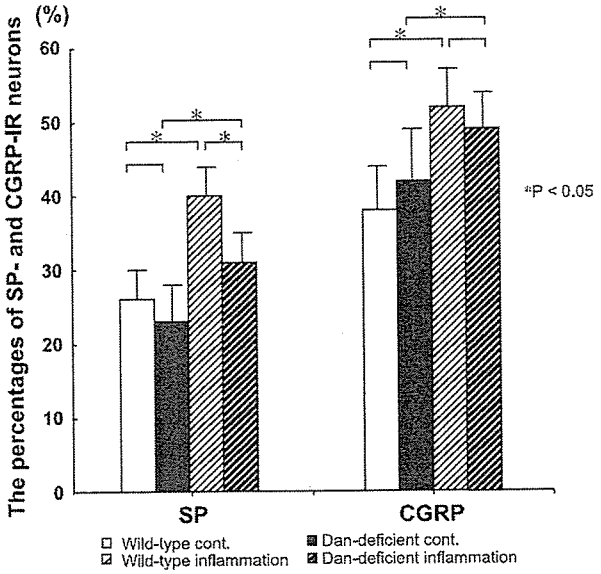

Fig. 7. The percentages of SP- and CGRP-IR DRG neurons were not significantly different between wild-type and Dan-deficient mice under normal conditions (day 0; wild type, SP: 26 ± 4%, CGRP, 38 ± 6%; Dan-deficient, SP: 23 ± 5%, CGRP, 42 ± 7%) (mean ± SE) ($P > 0.1$). Four days after inflammation, the ratios of SP- and CGRP-IR neurons in both types of mice were significantly increased compared with non-inflammatory control ($P < 0.05$). The ratio of SP-IR neurons in wild-type mice was higher than that in Dan-deficient mice ($P < 0.05$). However, there was no significant difference in the ratio of CGRP-IR neurons in both types of mice after inflammation ($P > 0.1$).

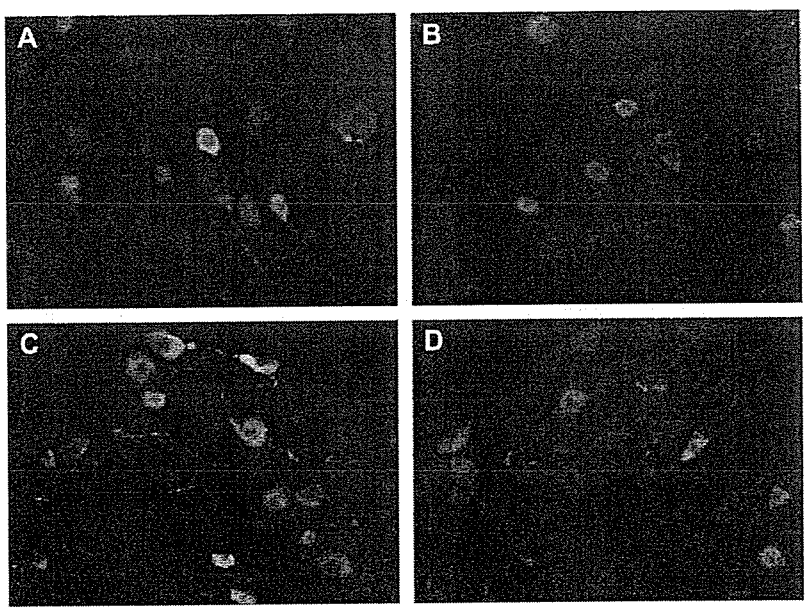

Fig. 6. Change in ratio of SP-IR DRG neurons of wild type (A, control group; C, inflammatory group) and Dan-deficient (B, control group; D, inflammatory group) mice after inflammation. SP was increased in wild-type and Dan-deficient mice after inflammation (C and D), however the number of SP-IR DRG neurons in wild-type mice (C) was significantly higher than that in Dan-deficient mice (D).

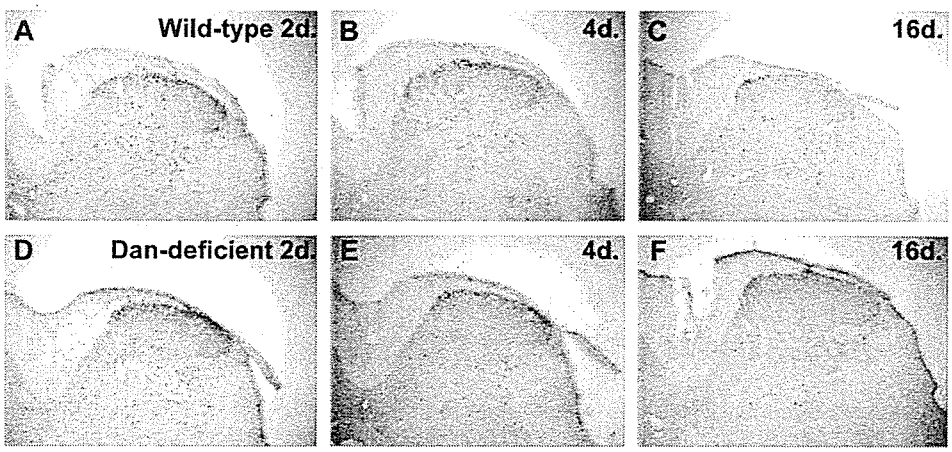

Fig. 8. Inflammation-induced Fos expression in the spinal dorsal horn in wild-type (A, B, and C) and Dan-deficient mice (D, E, and F). Fos-IR neurons in the superficial and deep laminae were observed at days 2 (A and D), 4 (B and E), and 16 (C and F) after CFA injection into the hind paw. More neurons were stained in wild-type mice than in Dan-deficient mice.

(Fig. 11). The amount of Fos expression in lamina I and II, 4 days after inflammation, was depressed by intrathecal injection of Dan antibody in wild-type mice ($P < 0.05$) (Figs. 10 and 11D). However, in the partial nerve injury models, the numbers of Fos-IR neurons following nerve injury in the superficial and deep laminae of Dan-deficient mice were not significantly different from those in wild-type mice ($P > 0.1$) (Fig. 11B).

It has been reported that noxious chemical and thermal stimulation of the skin leads to Fos expression in spinal dorsal horn neurons (Hunt et al., 1987). An increase of Fos expression in the spinal cord is observed following nerve injury in animal models (Catheline et al., 1999; Chi et al., 1993; Dai et al., 2001; Hudspith et al., 1999). The increase of Fos in the superficial and deep laminae may be related to hypersensitivity to noxious and innocuous stimuli following nerve injury (Catheline et al., 1999; Dai et al., 2001). After inflammation of the rat hind paw, noxious and innocuous stimuli induced a significantly large increase in Fos expression by dorsal horn neurons in laminae I–VI during lasting peripheral inflammation (Ma and Woolf, 1996).

In the current study, Fos expression was observed in superficial and deep laminae in the inflammatory and nerve injury models. We observed the same pattern, period, and location of spinal dorsal horn Fos expression as previously reported. Dan-deficient mice did not show significant hypersensitivity and mechanical allodynia caused by inflammation when compared with wild-type mice. However, the Dan-deficient mice showed hypersensitivity and mechanical allodynia caused by nerve injury. This finding was correlated with the decreased Fos expression observed in Dan-deficient mice under inflammatory conditions and with an insignificant difference in Fos expression after nerve injury when compared with wild-type mice.

Because Dan-IR nerve terminals were in the inner part of lamina II, the localization of Dan may lead to depression of Fos expression only in the inner part of lamina II in Dan-deficient mice. However, Fos expression was decreased in all superficial and deep laminae in the spinal dorsal horn. We postulate that the reason for this is as follows: it has been reported that NK1 receptor-immunoreactive neurons with cell bodies in lamina III or IV and dendrites that enter the superficial laminae also receive dense synaptic innervation from SP primary afferents (Todd et al., 2002). After inflammation of rat hind paw, Fos expression is more common in neurons with NK1 receptors. Therefore, a significant

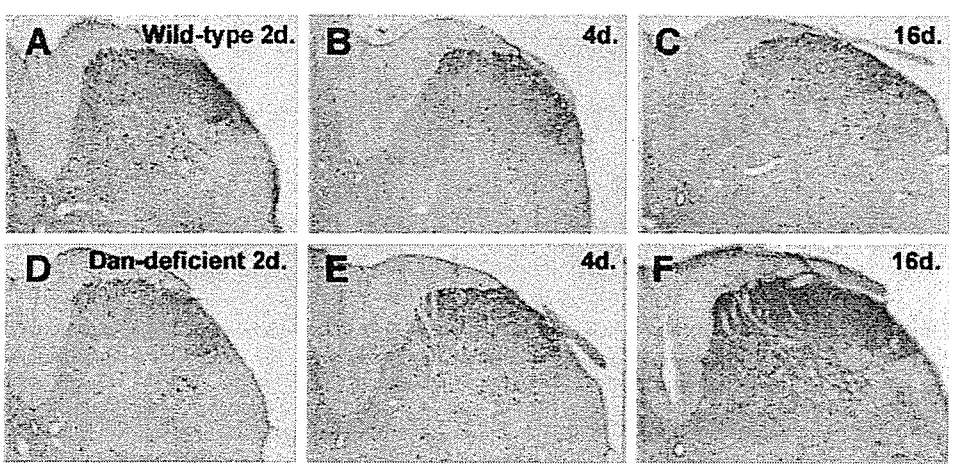

Fig. 9. Fos expression after nerve ligation in the spinal dorsal horn in wild-type (A, B, and C) and Dan-deficient mice (D, E, and F). The number of Fos-IR neurons at days 2 (A and D), 4 (B and E), and 16 (C and F) after nerve ligation was not significantly different between wild-type and Dan-deficient mice.

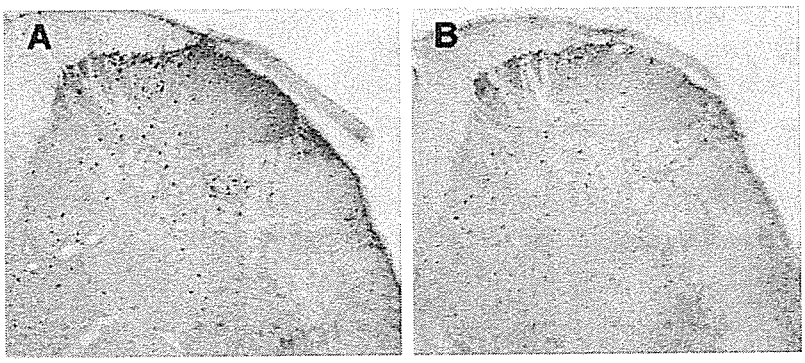

Fig. 10. Effect of intrathecally administered Dan monoclonal antibody on a CFA model of wild-type mice 4 days after inflammation. The level of Fos expression in superficial and deep layers 2 h after stimulation was depressed by intrathecal injection of Dan antibody in wild-type mice. (A, administration of mouse IgG; B, administration of Dan antibody).

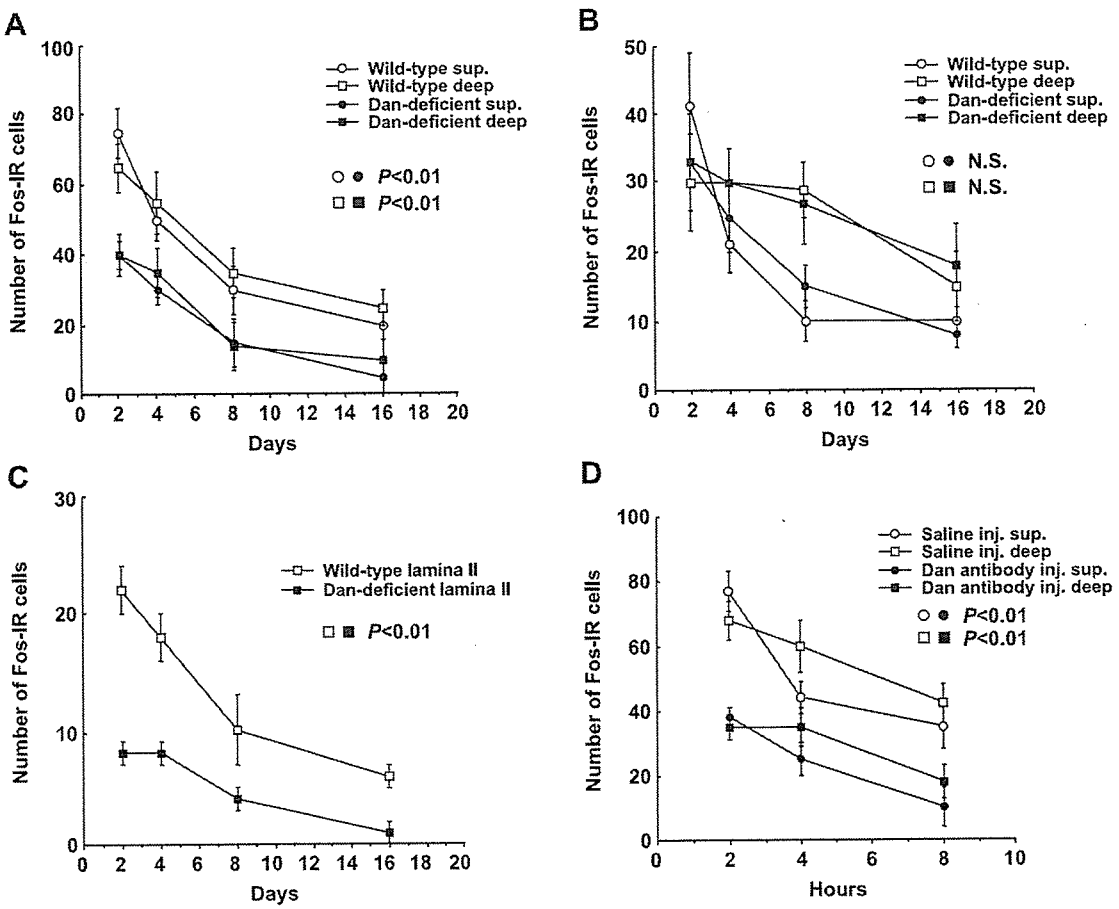

Fig. 11. Time course of Fos expression caused by inflammation in wild-type (open symbols) and Dan-deficient mice (solid symbols) (A). The numbers of Fos-IR cells in both laminae were less in Dan-deficient mice than in wild-type mice at all periods we observed ($P < 0.01$). In lamina II, immunoreacted for Dan, the number of Fos-IR cells was less in Dan-deficient mice (open square) than in wild-type mice (solid square) ($P < 0.01$) (C). Stimulation of the hind paw produced Fos in wild-type and Dan-deficient mice after nerve injury (B). On days 2, 4, 8, and 16, we did not observe significant differences in the numbers of Fos-IR cells in the superficial and deep laminae between both types of mice (open circle, wild-type superficial; open square, wild-type deep; solid circle, Dan-deficient superficial; solid square, Dan-deficient deep) ($P > 0.1$). The amount of Fos expression in superficial and deep layers 4 days after inflammation was depressed by intrathecal injection of Dan antibody in wild-type mice ($P < 0.05$) (Fig. 8D). Each point represents the time after stimulation of footpads (open circle, Fos expression in the superficial layers after IgG administration; open square, Fos expression in the deep layers after IgG administration; solid circle, Fos expression in the superficial layers after Dan-antibody administration; solid square, Fos expression in the deep layers after Dan-antibody administration).

proportion of these cell bodies in deep layers would be excited by noxious stimulation (Todd et al., 2002). SP was increased in the dorsal root ganglia, and the amount of these peptides in projections from the dorsal horn of the lumbar spinal cord would also be increased in inflammatory models (Schaible et al., 1994; Neumann et al., 1996; Noguchi et al., 1995). In the process, Dan is related to SP induction in DRG neurons after inflammation in the current study. We did not examine Dan receptors in the spinal cord. However, intrathecal-administered Dan suppressed pain behavior and Fos expression in superficial and deep layers of the spinal cord. We therefore propose that, except for SP induction in DRG, Dan also stimulates Fos in Dan-immunoreactive cells in the deep layer via the Dan-receptor pathway.

Experimental methods

The protocols for animal procedures in these experiments followed National Institutes of Health guidelines for the Care and Use of Laboratory Animals (1996 revision) and received approval from the ethics committees of our institutions.

Generation of Dan-deficient mice

A radio-labeled full-length mouse *Dan* cDNA was used to screen a mouse genomic library (λFIXII) by standard procedures. Genomic clones that gave a positive signal in the initial screening were digested with various combinations of restriction enzymes to verify that rearrangements had not occurred. The targeting construct was generated by replacing a 2.5-kb *Eco*RI–*Sma*I restriction fragment containing the exons II and III with an MC1-Neo cassette. An MC1-DT-A cassette was then inserted into the 3′side of the Neo cassette for negative selection. Forty micrograms of the linearized targeting vector were electroporated into 6×10^6 R1 ES cells, and the transfected cells were maintained in the presence of G418. Genomic DNA was prepared from the G418-resistant clones and subjected to Southern analysis using a radiolabeled *Sma*I–*Xba*I restriction fragment as a probe. Of 240 clones analyzed, two clones carried the desired mutant allele. These two targeted ES cell clones were then injected into BDF1 blastocysts to generate chimeric mice. Chimeras were mated with C57BL/6 females and lines were maintained by backcross onto C57BL/6 females.

Genotyping of mice at the Dan locus

Animals were genotyped either by Southern blot hybridization or by PCR-based analysis. For Southern analysis, mouse genomic DNA was digested completely with *Bam*HI, separated by 0.8% agarose gel electrophoresis, and transferred onto a nylon membrane filter. The filter was probed with the radiolabeled *Sma*I–*Xba*I restriction fragment. This strategy identified a 13-kb wild-type allele or a 1-kb targeted allele. PCR analysis was performed with the following primers: forward-1 (f1), 5′-ATACCTGCTTCCCCACTCCT-3′, reverse-1 (r1), 5′-GAACCTGCGTGCAATCCATCTT-3′; and forward-2 (f2), 5′-GACAAGAGTGCCTGGTGTGA-3′, reverse-2 (r2), 5′-GTGTTGGGGACGCTGTAACT-3′, which resulted in a 458-bp mutant type and a 227-bp wild-type product, respectively. The cycling conditions were 2 min at 98°C and 35 cycles of 30 s at 98°C, 30 s at 62°C, and 30 s at 72°C.

Inflammation model and nerve injury model

Forty-eight 12-week-old male Dan-deficient and wild-type mice were used. Under anesthesia with sodium pentobarbital (40 mg/kg, ip), 20 μl of complete Freund's adjuvant (CFA; 50 μg *Mycobacterium butyricum* in an oil-in-saline emulsion; Sigma, St. Louis, MO) was injected into the left hind paw. Partial sciatic nerve injury was caused by tight ligation of one-third to one-half of the left sciatic nerve.

Behavioral testing

The latency of paw withdrawal to thermal stimuli was measured as has been previously described (Hargreaves et al., 1988). Wild-type and Dan-deficient mice were placed in a planter test apparatus (UGO Basile; Camerio, Italy) consisting of a radiant heat source below an elevated floor of transparent glass. The radiant heat source beneath the glass floor was turned on, and the time between the start of stimulation and hind paw withdrawal was measured five times every 10 min. The average time for hind paw withdrawal was recorded. The level of tactile allodynia was estimated from 50% probability thresholds for paw withdrawal from mechanical stimuli using von Frey hairs, as previously described (Chaplan et al., 1994).

Time course of Fos expression in CFA and nerve injury models

Touch-evoked increases in Fos expression were examined from 2 to 16 days after CFA injection or nerve injury to wild-type (n = 24) and Dan-deficient mice (n = 24). Gentle touch stimuli were applied manually to the injected plantar surface of these animals with the flat surface of the experimenter's thumb, as described in detail previously (Sivilotti and Woolf, 1994). Each touch, lasting 2 s and moving from the middle position of the foot to the distal footpad, was applied once every 4 s for 10 min under halothane anesthesia.

We examined the effect of intrathecally administered mouse monoclonal antibody to Dan (5 μg) (Chiba Cancer Center Research Institute) on the CFA model in wild-type mice 4 days after inflammation (n = 12). To administer antibodies intrathecally, a 30-gauge needle was inserted into the intralamina space between L6 and S1. Stimulation of the footpad was applied after intrathecal injection of Dan antibody. To obtain control data, 5 μg of mouse IgG_1 was administered (n = 12). The number of Fos-immunoreactive (IR) cells in the spinal cord was evaluated 2, 4, and 8 h after stimulation.

Immunohistochemistry

Mice were anesthetized with 3% halothane and perfused transcardially with 100 ml of 4% paraformaldehyde (PFA) in phosphate buffer (0.1 M, pH 7.4). The spinal cord was resected at the level of C4 and L5, and the L5 dorsal root ganglia (DRGs) and footpad were removed and 20-μm sections cut on a cryostat. To examine axonal transport of Dan from DRG to the spinal dorsal horn, the spinal cord at the level of L4 was resected 2 weeks after dorsal root section. Sections were incubated in a blocking solution containing 0.3% Triton X-100 and 5% skim milk in 0.01 M phosphate-buffered saline (PBS) for 90 min at room temperature. Sections were processed immunohistochemically using a free-floating avidin–biotin complex (ABC) technique by incubating them with rabbit antibody to Dan (1:1000 in blocking solution), substance P

(SP) (1:100; Zymed, San Francisco, CA), calcitonin gene-related protein (CGRP) (1:2000; Chemicon, Temecula, CA), neurokinin receptor (NK1) (Dr. R. Shigemoto, Kyoto University, Japan), or Fos (1:1000; Santa Cruz Biotechnology, Santa Cruz, CA) for 20 h at 4 °C, followed by incubation with biotinylated goat anti-rabbit IgG (Vector Labs, Burlingame, CA; 1:100 in blocking solution) and fluorescein isothiocyanate (FITC) avidin D (1:100; Vector Labs). For Fos immunostaining of the spinal cord, after incubation with an avidin–biotin enzyme complex (Vector Labs; 1:100 in blocking solution) for 90 min at room temperature, immunoreaction was visualized using an ammonium nickel sulfate enhanced diaminobenzidine (DAB) reaction. We counted cells in 7 serial sections of the DRG and 10 sections of the spinal cord. The number of Dan-, SP-, and CGRP-IR neurons in the DRG, and Fos-IR neurons in the laminae I, II, and those in the deep layers (laminae III–VI) were counted.

Double-labeling immunohistochemistry

After incubation with rabbit antibody to Dan for 20 h at 4 °C, sections were incubated with goat anti-rabbit Alexa 488 (FITC) (1:400; Molecular Probes Inc., Eugene, OR).

Sections were incubated with mouse antibody to CGRP (marker for peptergic small neurons; 1:2000; Chemicon, Temecula, CA), isolection B4 (IB4; marker for non-peptidergic small neurons; 1:1000; Chemicon, Temecula, CA), guinea pig antibody to P2X3 (marker for non-peptidergic small neurons; 1:2000; Neuromic, Minneapolis, MN), or mouse antibody to neurofilament 200 (NF200; marker for myelinated A fiber s neurons; 1:1000; Chemicon, Temecula, CA) for 20 h at 4 °C CGRP, isolectin B4, P2X3 and NF200 were visualized by following incubation with goat anti-mouse Alexa 594 (Texas red; 1:400), streptavidin Alexa 594 (Texas red; 1:400), goat anti-guinea pig Alexa 594 (Texas red; 1:400), and goat anti-mouse Alexa 594 (Texas red; 1:400), respectively.

Statistical analysis

The differences among the groups were compared using ANOVA. Differences were considered to be statistically significant at $P < 0.05$.

Acknowledgments

We thank Dr. R. Shigemoto (Kyoto University) for the gift of antibody to NK1 and K. Kitajo for technical assistance.

References

Abbadie, C., Brown, J.L., Mantyh, P.W., Basbaum, A.I., 1996. Spinal cord substance P receptor immunoreactivity increases in both inflammatory and nerve injury models of persistent pain. Neuroscience 70, 201–209.

Ai, X., Cappuzzello, J., Hall, A.K., 1999. Activin and bone morphogenetic proteins induce calcitonin gene-related peptide in embryonic sensory neurons in vitro. Mol. Cell. Neurosci. 14, 506–518.

Bradbury, E.J., Burnstock, G., McMahon, S.B., 1998. The expression of P2X3 purinoreceptors in sensory neurons: effects of axotomy and glial-derived neurotrophic factor. Mol. Cell. Neurosci. 12, 256–268.

Catheline, G., Le Guen, S., Honore, P., Besson, J.M., 1999. Are there long-term changes in the basal or evoked Fos expression in the dorsal horn of the spinal cord of the mononeuropathic rat? Pain 80, 347–357.

Chaplan, S.R., Bach, F.W., Pogrel, J.W., Chung, J.M., Yaksh, T.L., 1994. Quantitative assessment of tactile allodynia in the rat paw. J. Neurosci. Methods 53, 55–63.

Chi, S.I., Levine, J.D., Basbaum, A.I., 1993. Effects of injury discharge on the persistent expression of spinal cord *fos*-like immunoreactivity produced by sciatic nerve transection in the rat. Brain Res. 617, 220–224.

Dai, Y., Iwata, K., Kondo, E., Morimoto, T., Noguchi, K., 2001. A selective increase in Fos expression in spinal dorsal horn neurons following graded thermal stimulation in rats with experimental mononeuropathy. Pain 90, 287–296.

Dionne, M.S., Skarnes, W.C., Harland, R.M., 2001. Mutation and analysis of Dan, the founding member of the Dan family of transforming growth factor beta antagonists. Mol. Cell. Biol. 21, 636–643.

Donnerer, J., Schuligo, I.R., Stein, C., 1992. Increased content and transport of substance P and calcitonin gene-related peptide in sensory nerves innervating inflamed tissue: evidence for a regulatory function of nerve growth factor in vivo. Neuroscience 49, 693–698.

Hargreaves, K., Dubner, R., Brown, F., Flores, C., Joris, J., 1988. A new and sensitive method for measuring thermal nociception in cutaneous hyperalgesia. Pain 32, 77–88.

Hudspith, M.J., Harrisson, S., Smith, G., Bountra, C., Elliot, P.J., Birch, P.J., Hunt, S.P., Munglani, R., 1999. Effect of post-injury NMDA antagonist treatment on long-term *fos* expression and hyperalgesia in a model of chronic neuropathic pain. Brain Res. 822, 220–227.

Hsu, D.R., Economides, A.N., Wang, X., Eimon, P.M., Harland, R.M., 1998. The *Xenopus* dorsalizing factor Gremlin identifies a novel family of secreted proteins that antagonize BMP activities. Mol. Cell 1, 673–683.

Hunt, S.P., Pini, A., Evan, G., 1987. Induction of c-*fos*-like protein in spinal cord neurons following sensory stimulation. Nature 328, 632–634.

Liu, T., Tracey, D.J., 2000. ATP P2X receptors play little role in the maintenance of neuropathic hyperalgesia. NeuroReport 11, 1669–1672.

Llewellyn-Smith, I.J., Burnstock, G., 1998. Ultrastructural localization of P2X3 receptors in rat sensory neurons. NeuroReport 9, 2545–2550.

Ma, Q.P., Woolf, C.J., 1996. Basal and touch-evoked *fos*-like immunoreactivity during experimental inflammation in the rat. Pain 67, 307–316.

Malmberg, A.B., Chen, C., Tonegawa, S., Basbaum, A.I., 1997. Preserved acute pain and reduced neuropathic pain in mice lacking PKCgamma. Science 278, 279–283.

McCarson, K., Krause, J.E., 1994. NK-1 and NK-3 type tachykinin receptor mRNA expression in the rat spinal cord dorsal horn is increased during adjuvant or formalin induced nociception. J. Neurosci. 14, 712–720.

Neumann, S., Doubell, T.P., Leslie, T., Woolf, C.J., 1996. Inflammatory pain hypersensitivity mediated by phenotypic switch in myelinated primary sensory neurons. Nature 384, 360–364.

Noguchi, K., Ruda, M.A., 1992. Gene regulation in an ascending nociceptive pathway: inflammation-induced increase in preprotachykinin mRNA in rat lamina I spinal projection neurons. J. Neurosci. 12, 2563–2572.

Noguchi, K., Kawai, Y., Fukuoka, T., Senba, E., Miki, K., 1995. Substance P induced by peripheral nerve injury in primary afferent sensory neurons and its effect on dorsal column nucleus neurons. J. Neurosci. 11, 7633–7643.

Noguchi, K., Morita, Y., Kiyama, H., Ono, K., Tohyama, M., 1988. A noxious stimulus induces the preprotachykinin-A gene expression in the rat dorsal root ganglion: a quantitative study using in situ hybridization histochemistry. Brain Res. 464, 31–35.

Ohtori, S., Yamamoto, T., Ino, H., Hanaoka, E., Shinbo, J., Ozaki, T., Takada, N., Nakamura, Y., Chiba, T., Nakagawara, A., Sakiyama, S., Sakashita, Y., Takahashi, K., Tanaka, K., Yamagata, M., Yamazaki, M., Shimizu, S., Moriya, H., 2002. Differential screening-selected gene aberrative in neuroblastoma protein modulates inflammatory pain in the spinal dorsal horn. Neuroscience 110, 579–586.

Ozaki, T., Sakiyama, S., 1993. Molecular cloning and characterization of a cDNA showing negative regulation in v-*src*-transformed 3Y1 rat fibroblasts. Proc. Natl. Acad. Sci. U. S. A. 90, 2593–2597.

Ozaki, T., Sakiyama, S., 1994. Tumor-suppressive activity of N03 gene product in v-*src*-transformed rat 3Y1 fibroblasts. Cancer Res. 54, 646–648.

Ozaki, T., Nakamura, Y., Enomoto, H., HilRose, M., Sakiyama, S., 1995. Overexpression of DAN gene product in normal rat fibroblasts causes a retardation of the entry into the S phase. Cancer Res. 55, 895–900.

Pearce, J.J., Penny, G., Rossant, J., 1999. A mouse cerberus/Dan-related gene family. Dev. Biol. 209, 98–110.

Piccolo, S., Agius, E., Leyns, L., Bhattacharyya, S., Grunz, H., Bouwmeester, T., De Robertis, E.M., 1999. The head inducer Cerberus is a multifunctional antagonist of Nodal. BMP and Wnt signals. Nature 397, 707–710.

Schaible, H.G., Freudenberger, U., Neugebauer, V., Stiller, R.U., 1994. Intraspinal release of immunoreactive calcitonin gene-related peptide during development of inflammation in the joint in vivo-a study with antibody microprobes in cat and rat. Neuroscience 62, 1293–1305.

Sivilotti, L., Woolf, C.J., 1994. The contribution of GABAA and glycine receptors to central sensitization: disinhibition and touch-evoked allodynia in the spinal cord. J. Neurophysiol. 72, 169–179.

Stanfa, L.C., Kontinen, V.K., Dickenson, A.H., 2000. Effects of spinally administered P2X receptor agonists and antagonists on the responses of dorsal horn neurones recorded in normal, carrageenan-inflamed and neuropathic rats. Br. J. Pharmacol. 129, 351–359.

Stanley, E., Biben, C., Kotecha, S., Fabri, L., Tajbakhsh, S., Wang, C.C., Hatzistavrou, T., Roberts, B., Drinkwater, C., Lah, M., Buckingham, M., Hilton, D., Nash, A., Mohun, T., Harvey, R.P., 1998. DAN is a secreted glycoprotein related to *Xenopus* cerberus. Mech. Dev. 77, 173–184.

Todd, A.J., Puskar, Z., Spike, R.C., Hughes, C., Watt, C., Forrest, L., 2002. Projection neurons in lamina I of rat spinal cord with the neurokinin 1 receptor are selectively innervated by substance P-containing afferents and respond to noxious stimulation. J. Neurosci. 22, 4103–4113.

Identification of novel human neuronal leucine-rich repeat (h*NLRR*) family genes and inverse association of expression of *Nbla10449/*h*NLRR-1* and *Nbla10677/*h*NLRR-3* with the prognosis of primary neuroblastomas

SHIHO HAMANO[1,2], MIKI OHIRA[1], ERIKO ISOGAI[1], KOUNOSUKE NAKADA[2] and AKIRA NAKAGAWARA[1]

[1]Division of Biochemistry, Chiba Cancer Center Research Institute, 666-2 Nitona, Chuoh-ku, Chiba 260-8717; [2]Division of Pediatric Surgery, St. Marianna University School of Medicine, 2-16-1 Sugao, Miyamae-ku, Kawasaki 216-8511, Japan

Received August 1, 2003; Accepted September 24, 2003

Abstract. To search for novel prognostic indicators, we previously cloned >2,000 novel genes from primary neuroblastoma (NBL) cDNA libraries and screened for differential expression between the subsets with favorable (stage 1 or 2 with a single copy of *MYCN*) and unfavorable (stage 3 or 4 with amplification of *MYCN*) prognosis. From them, we have identified 3 genes of human neuronal leucine-rich repeat protein (NLRR) family: *Nbla10449/*h*NLRR-1*, *Nbla00061/*h*NLRR-2/GAC1* and *Nbla10677/*h*NLRR-3*. An additional family member, h*NLRR-5*, was also found by homology search against public database. NLRR family proteins have been proposed to function as a neuronal adhesion molecule or soluble ligand binding receptor like *Drosophila toll* and *slit* with multiple domains including 11 sets of extracellular leucine-rich repeat (LRR)-motifs. However, the functional role of the NLRR protein family has been elusive. Our present study shows that h*NLRR* mRNAs are preferentially expressed in nervous system and/or adrenal gland. In cancer cell lines, h*NLRR-1*, h*NLRR-3* and h*NLRR-5* are expressed at high levels in the neural crest-derived cells. Most remarkably, in primary NBLs, h*NLRR-1* is significantly expressed at high levels in unfavorable subsets as compared to favorable ones, whereas the expression pattern of h*NLRR-3* and h*NLRR-5* is the opposite. In order to understand the function of these receptors, we have used newborn mouse superior cervical ganglion (SCG) cells which are dependent on nerve growth factor (NGF) for their survival. Expression of the mouse counterparts of h*NLRR-2* and h*NLRR-3* is up-regulated after NGF-induced differentiation and down-regulated after NGF depletion-induced apoptosis. On the other hand, expression of h*NLRR-1* and h*NLRR-5* is inversely regulated in the same system. These results have suggested that the regulation of the h*NLRR* family genes may be associated with NGF signaling pathway in both SCG cells and neuroblastoma. Our quantitative real-time RT-PCR analysis using 99 primary NBLs has revealed that high levels of h*NLRR-1* expression are significantly associated with older age (>1 year, p=0.0001), advanced stages (p=0.0007), low expression of *TrkA* (p=0.011), and *MYCN* amplification (p=0.0001), while those of h*NLRR-3* expression are significantly correlated with the favorable prognostic indicators. Furthermore, multivariate analysis reveals that expression of h*NLRR-1* is an independent prognostic indicator in human neuroblastoma. Thus, our results demonstrate that, despite being members of the same family, h*NLRR-1* and h*NLRR-3* may share different biological function among the NBL subsets, and that their expression level becomes novel prognostic indicators of NBL.

Correspondence to: Dr Akira Nakagawara, Division of Biochemistry, Chiba Cancer Center Research Institute, 666-2 Nitona, Chuoh-ku, Chiba 260-8717, Japan
E-mail: akiranak@chiba-ccri.chuo.chiba.jp

Key words: leucine-rich repeat, neuroblastoma, differential expression, prognostic factor

Introduction

Neuroblastoma (NBL) is one of the most common pediatric tumors originating from sympathoadrenal lineage of the neural crest. NBL shows variable biological behavior which characterizes different clinical subsets (1). The tumors found in young children, <1 year of age usually regress spontaneously, while those in the older children are often aggressive leading to poor outcome. Recent advances in molecular biology have identified the important molecules involved in the regulation of growth, differentiation and programmed cell death during development of the sympathoadrenal cells (2), some of which link to the modulation of NBL biology. These include Trk family tyrosine kinase receptors and *MYCN* proto-oncogene. TrkA, a high-affinity receptor for nerve growth factor (NGF), is expressed in favorable subsets of NBL and regulates differentiation and/or regression of the tumor cells (3). On the other hand, TrkB, a receptor for brain-derived neurotrophic factor (BDNF) and neurotrophin-4 (NT-4), is expressed in NBLs with unfavorable prognosis. An autocrine loop of BDNF/NT-4 and TrkB may promote tumor cell survival and increase their invasiveness (4). Amplification of *MYCN* is significantly associated with allelic loss of the

distal region of chromosome 1, and both are indicators of poor prognosis. A recent report suggests that *MYCN* oncoprotein induces expression of *Id-2* with a helix-loop-helix domain and in turn negatively regulates Rb tumor suppressor in NBL (5). However, many important genes may still be missing for better understanding of NBL biology as well as predicting the prognosis. In order to identify novel NBL-related genes and promote better understanding of the molecular mechanism of NBL genesis and its biology, differential screening method has been applied (6).

We have previously constructed full-length-enriched oligocapping cDNA libraries from different subsets of primary NBL (6,7). One derived from the mixture of favorable NBLs in stage 1 with single-copy of *MYCN*, and the other from unfavorable NBLs in stage 3 and 4 with *MYCN* amplification. We have finished end-sequencing of 2,500 clones obtained from each library, and found that the expression profile is markedly different between the subsets. So far, 1,800 independent genes from these libraries have been subjected to semi-quantitative RT-PCR using 16 favorable and 16 unfavorable NBLs to find the genes differentially expressed between favorable (F) and unfavorable (UF) subsets (8,9).

In this study, we have identified novel human *NLRR* family genes that are differentially expressed among the NBL subsets. NLRRs are proteins with leucine-rich repeat (LRR) domains which may be involved in protein-protein interactions (10). They may also function as cell-adhesion molecules or signaling receptors implicated in regulation of the neural development. Expression of the h*NLRR-1/Nbla10449* gene is significantly associated with short survival as well as conventional poor-prognostic factors, whereas that of the h*NLRR-3/Nbla10677* gene is increased in favorable subset of NBL. Our results suggest that the differential expression of h*NLRR* genes among the NBL subsets is involved in the regulation of growth, differentiation and cell death of human NBL.

Materials and methods

Patients. We studied tumors from 99 children with NBL diagnosed between 1995-1999. Fifty-four Japanese patients were identified by a mass screening program started in 1985 (9,10). The selection of tumors for this study was solely based on the availability of a sufficient amount of tumor tissue, from which DNA and mRNA could be prepared for the analyses described below.

The diagnosis of NBL was confirmed by histologic assessment of the tumor specimen obtained at surgery according to the classification of Shimada *et al* (11). There were 57 tumors with favorable histology, and 42 with unfavorable histology. The tumors were staged according to the International Neuroblastoma Staging System (INSS) (12). Thirty-eight tumors (36 identified by mass screening) were stage 1, 14 (11 identified by mass screening) stage 2, 5 (3 identified by mass screening) stage 4s, 10 (3 identified by mass screening) stage 3, and 32 (1 identified by mass screening) stage 4. The patients were treated according to the protocols previously described (13).

Tumor samples and cell lines. Fresh, frozen tumorous tissues were sent to the Division of Biochemistry, Chiba Cancer Center Research Institute, from various hospitals in Japan with informed consent from the patient's parents. All samples were obtained by surgery (or biopsy) and stored at -80°C. Studies were approved by the Institutional Review Board of the Chiba Cancer Center. Human cell lines which we used included NBL (CHP134, CHP901, GANB, GOTO, IMR32, SMS-KAN, SMS-KCN, KP-N-NS, LAN-5, NB-1, NB-9, NBKM-1, NB (Tu)-1, NLF, NMB, RTBM1, SMS-SAN, SK-N-BE, SK-N-DZ, TNB, TGW, LHN, NGP, NB69, NBL-S, OAN, SK-N-AS, SK-N-SH, SH-SY5Y, and CNB-RT), osteosarcoma (OST, Saos2, and NOS1), rhabdomyosarcoma (RMS-MK and ASPS-KY), colorectal adenocarcinoma (COLO320, SW480, and LOVO), a hepatocellular cancer (HepG2), breast cancer (MOA-MB-453 and MB231), melanoma (G361, G32TG, A875), a thyroid cancer (TTC11), a gastric cancer (KATO3), esophageal cancer (ECGI10), a pancreatic cancer (ASPC1) and a lung cancer cell lines (A549). The cells were cultured in the RPMI-1640 medium (Nissui Pharmaceutical Co. Ltd., Tokyo) with 10% fetal bovine serum and 50 μg/ml penicillin/streptomycin at humidified 5% CO_2/95% air at 37°C.

Primary culture of newborn mouse superior cervical ganglion cells. The SCG neurons were isolated from newborn mice, and treated with 50 ng/ml of NGF for 5 days, as previously reported (14). RNAs were isolated 12, 24, and 48 h after depleting NGF and adding anti-NGF antibody (1% v/v).

Northern blot analysis. Multiple Tissue Northern blot purchased from Clontech (Palo Alto, CA, USA) was used for Northern analysis with cDNA fragments labeled with α-[^{32}P]dCTP as probes. Hybridization was performed in the ExpressHyb hybridization buffer (Clontech) at 68°C for 1 h. Membrane was washed twice in 2X SSC/0.05% SDS at room temperature for 30 min, twice in 0.1X SSC/0.1% SDS at 50°C for 40 min. After washing, the filter was autoradiographed with X-ray film. The membrane was boiled in 0.1% SDS for 10 min for reprobing, and rehybridized with ß-actin as a control.

Semi-quantitative RT-PCR. cDNA was synthesized from 5 μg of total RNA in a 20 μl reaction mixture containing 200 units of Superscript II reverse transcriptase (Life Technologies, Inc.) and pd(N)$_6$ random hexamer (Takara Shuzo Co., Ltd., Ohtsu, Japan). The resulting cDNA fragments were diluted to be a 1:10 solution for PCR templates. The following pairs of forward and reverse primer sets were prepared for amplification: *NLRR-1*, 5'-GTCGATGTCCATGAATACAACCT-3' and 5'-CAAGGCTAATGACGGCAAAC-3'; *NLRR-2*, 5'-TGACCTATTCCTGACGG-3' and 5'-AAATCACAGTCTCGGGC-3'; *NLRR-3*, 5'-ACTCTTGCCTAATACCCTGAC-3' and 5'-AGATGGTATTCGAGCACTTTG-3'; *GAPDH*, 5'-CTGCACCAACAATATCCC-3' and 5'-GTAGAGACAGGGTTTCAC-3'. All PCR amplifications were performed with a Perkin-Elmer Corp. GeneAmp PCR 9700, using rTaq polymerase (Takara Shuzo Co., Ltd.) with 35 cycles of sequential denaturation (95°C for 15 sec) and annealing-extension (58°C for 15 sec and 72°C for 1 min). *GAPDH* was used as a control and amplified under the same condition except for reduced amplification cycles to 28. PCR templates

were standardized by its *GAPDH* expression before performing semi-quantitative PCR. The products were electrophoresed on 2.0% agarose gels and stained with ethdium bromide for visualization.

Quantitative real-time RT-PCR. cDNA was prepared by the same method as in the semi-quantitative RT-PCR and 2 µl of the 40-fold dilution was used for each PCR reaction. Primers and TaqMan probes for *Nbla10449* and *Nbla10677* were designed using the primer design software Primer Express™ (Perkin-Elmer Applied Biosystems). TaqMan GAPDH control reagent kit (Perkin-Elmer Applied Biosystems) was used for *GAPDH* expression as a control. Reaction mixture (25 µl), containing 2 µl of cDNA, 1X TaqMan mixture, 0.3 µM forward and reverse primers, and 0.2 µM TaqMan probe were used for PCR. The condition of PCR was as follows: 2 min at 50°C (stage 1), 10 min at 95°C (stage 2), and then 50 cycles of amplification for 15 sec at 95°C and 1 min at 60°C (stage 3).

Statistical analysis. The student's t-tests were used to explore possible associations between *Nbla10449/hNLRR-1* expression and other factors, such as age. Since the values of the *Nbla10449/hNLRR-1* and *Nbla10677/hNLRR-3* expression were skewed, a log transformation was used to achieve the normality when using t-test and Cox regression. The distinction between high and low levels of *Nbla10449* was based on the median value (low, *Nbla10449* <0.31 d.u.; high, Nbla10449 >0.31 d.u.), regardless of tumor stage, *MYCN* copy number, or survival. The distinction between high and low levels of *Nbla10677* was based on the median value (low, *Nbla10677* <1.04 d.u.; high, *Nbla10677*>1.04 d.u.), regardless of tumor stage, *MYCN* copy number, or survival. Kaplan-Meier survival curves were calculated, and survival distributions were compared using the log-rank test. Cox regression models were used to explore associations between *Nbla10449/Nbla10677*, age, *MYCN* copy number, mass screening, tumor origin and survival. Statistical significance was declared if the p value was <0.05. Statistical analysis was performed using Stata 6.0. (Stata Statistical Software: Release 6.0 College Station, Stata Corporation, TX, 1999).

Results

Identification of novel human homologues of NLRR family genes, Nbla10449/hNLRR-1 and Nbla10677/hNLRR-3, and their differential expression between favorable and unfavorable subsets of neuroblastoma. To identify the genes differentially expressed between favorable and unfavorable NBLs, semi-quantitative RT-PCR analyses were performed. Sixteen favorable (F) and 16 unfavorable (UF) NBLs were used as PCR templates after normalization by GAPDH expression. So far, ~1,800 independent genes from the NBL cDNA libraries have been surveyed, resulting in the approximately 300 genes with differential expression between the subsets (8,9). Among them, we found *Nbla10449* and *Nbla10677* genes that are highly homologous to the mouse *NLRR-1* and *NLRR-3* genes, respectively. *Nbla10449/hNLRR-1* was preferentially expressed in UF NBLs, whereas *Nbla10677/hNLRR-3* was highly expressed in F NBLs (Fig. 3A).

Full-length cDNA cloning and structure of human NLRR-1, NLRR-2, NLRR-3 and NLRR-5 genes. We performed sequencing of whole inserts of *Nbla10449* and *Nbla10677* and defined their full-length cDNA sequences. In addition, during the process, we also identified human *NLRR-5* by homology search on the database. Furthermore, the other clone, *Nbla00061*, was found to be the same gene as *GAC1* which we renamed as h*NLRR-2*. *NLRR-4* has recently been reported by another group (15).

Nbla10449/hNLRR-1. A full-length *Nbla10449* genes comprised 3,060 bp, with an open reading frame (ORF) of 2,151 bp. The deduced protein was 716 a.a. in length, and included 2 hydrophobic stretches corresponding to a signal peptide at the extreme N-terminal region and a deduced transmembrane domain close to the C-terminal region (Fig. 1A). Analysis of the extracellular domain revealed the presence of 11 leucine-rich repeats encompassed by flanking cystein cluster, a leucine-rich repeat N-terminal domain (LRRNT) and a leucine-rich repeat C-terminal domain (LRRCT), a single immunogloblin C2 type domain, and a fibronectin type III domain (Fig. 1). Homology search against public database showed that *Nbla10449* was identical to the human *EST KIAA1497* (GenBank/DDBJ accession number AB040930) which lacked the N-terminal region and was similar to 2 leucine-rich repeat proteins, m*NLRR-1* (acc. no. D45913) and *Xenopus* x*NLRR-1* (acc. no. AB014462). The identities of deduced Nbla10449 protein to mNLRR-1 and xNLRR-1 were 92 and 75%, respectively. We also analyzed genomic structure of *Nbla10449*, and found that this gene comprised of single exon without any intron and mapped to chromosome 3p region.

Nbla10677/hNLRR-3. Nbla10677 comprised 2,471 bp with an ORF of 2,127bp (acc. no. AB060967) without intron, and mapped to chromosome 7q31. The deduced protein contained 708 a.a. and had a similar structure to Nbla10449/hNLRR-1 (Fig. 1A). In addition, the RGD sequence, an integrin-binding domain, was found in the leucine-rich repeats. Homology search showed that *Nbla10677* was identical to human cDNA FLJ11129 (acc. no. AK001991) and highly similar to the leucine-rich repeat proteins of mouse (mNLRR-3; acc. no. D49802) and rat (rNLRR-3; acc. no. AF291437). Therefore, Nbla10677 seemed to be a human NLRR-3. The Nbla10677/hNLRR-3 showed 85 and 83% similarity to mNLRR-3 and rNLRR-3 proteins, respectively.

Nbla00061/GAC1/hNLRR-2. The *Nbla00061* cDNA clone comprised 3,206 bp including a partial ORF of 2,142 bp. Sequence analysis revealed that it is identical to a *glioma amplified on chromosome 1* gene, *GAC1* (acc. no. AF030435), mapped to chromosome 1q32.1. The GAC1 protein, which was previously reported to be a member of an NLRR protein family (15), had 713 a.a. with a similar structure to NLRR-1 and 3 (Fig. 1). GAC1 showed 98% identity to mNLRR-2, although the latter was reported as only a partial sequence (16). It showed only 54 and 50% identities to mNLRR-1 and mNLRR-3, respectively, indicating that Nbla00061/GAC1 is a human counterpart of mNLRR-2.

m*NLRR-4* was cloned by another group from hemangioblast-like cell line derived from E11.5 mouse AGM and its predicted protein has 4 LRRs, fibronectin 3 and EGF-like motives in the extracellular region (Rump A *et al*, The Molecular Biology Society of Japan Conference, Yokohama,

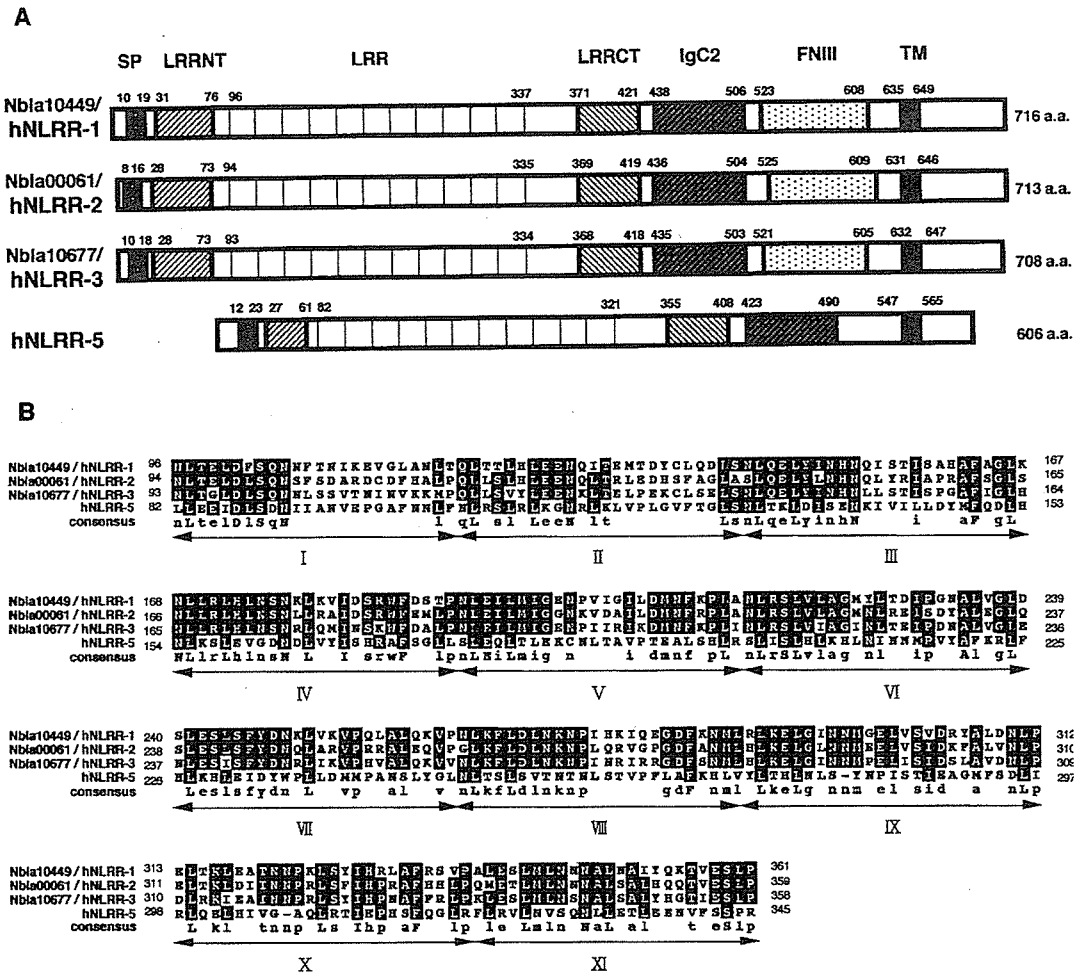

Figure 1. Structures and deduced amino acid sequences of hNLRR families. A, Schematic representation of hNLRR-1, hNLRR-2, hNLRR-3 and hNLRR-5 whose proteins consist of 716, 713, 708 and 606 a.a., respectively. SP, predicted signal peptide; TM, predicted transmembrane region; LRRNT, leucine-rich repeat N-terminal domain; LRRCT, leucine-rich repeat C-terminal domain; LRR, leucine-rich repeat; Igc2, immunoglobulin C-2 type domain; FN III, fibronectin type III domain. B, Amino acid alignment of the LRR domains of hNLRR families. Eleven repeats of LRR motif are shown by Roman numerals. Consensus sequences are highlighted and shown below.

abs. 4P-500 and 4P-501, 2001). h*NLRR-5* has no EGF-like motif and has 11 LRRs, and we failed to identify its human counterpart in the database or our NBL cDNA libraries.

h*NLRR-5*. Homology search against proteins deduced from genomic sequences on chromosome 9p revealed the presence of another family member of NLRR (acc. no. CAC22713). Its deduced protein was 606 a.a. in length and had a similar structure to the other NLRR members. However, a fibronectin domain was not included in this product. It showed 56 and 53% identities to mouse hypothetical protein (acc. no. BAB32403) and *Macaca fascicularis* hypothetical protein (acc. no. BAB03557), respectively, suggesting that they were mouse and *Macaca fascicularis* counterparts of hNLRR-5.

Expression of hNLRR family genes in human tissues. To examine whether *hNLRR* genes display neuron-specific expression, Northern analysis and semi-quantitative RT-PCR were performed. Among several human fetal tissues, h*NLRR-1*, h*NLRR-2* and h*NLRR-3* mRNAs were strongly expressed in brain at the size of 4.0-4.5 kb (Fig. 2A). By contrast, h*NLRR-5* was ubiquitously expressed in all main fetal organs. The size of h*NLRR-2* transcript in the liver was smaller than that in the other tissues. In adult human tissues, all h*NLRR-1*, h*NLRR-2*, h*NLRR-3* and h*NLRR-5* were also preferentially expressed at high levels in the nerve tissues (Fig. 2B).

Expression of hNLRR family genes in neuroblastoma and cell lines. Expression of h*NLRR* family genes was measured in primary neuroblastomas and cell lines using semi-quantitative RT-PCR. As shown in Fig 3A, *Nbla10449/hNLRR-1* was highly expressed in UF NBLs, whereas *Nbla10677/hNLRR-3* and h*NLRR-5* were preferentially expressed in the F NBLs. *Nbla00061/hNLRR-2* seemed to be equally expressed between both subsets. In NBL cell lines, expression of *NLRR-1* was observed relatively more frequently in the lines with *MYCN* amplification than in those with a single copy of the gene. On the other hand, *NLRR-3* appeared to be expressed rather frequently in the cell lines without *MYCN* amplification. Interestingly, however, there was a tendency that the cells with high expression of *NLRR-1* also had a high levels of expression of *NLRR-3* (Fig. 3B). The expression of both h*NLRR-2* and h*NLRR-5* was found in most NBL cell lines.

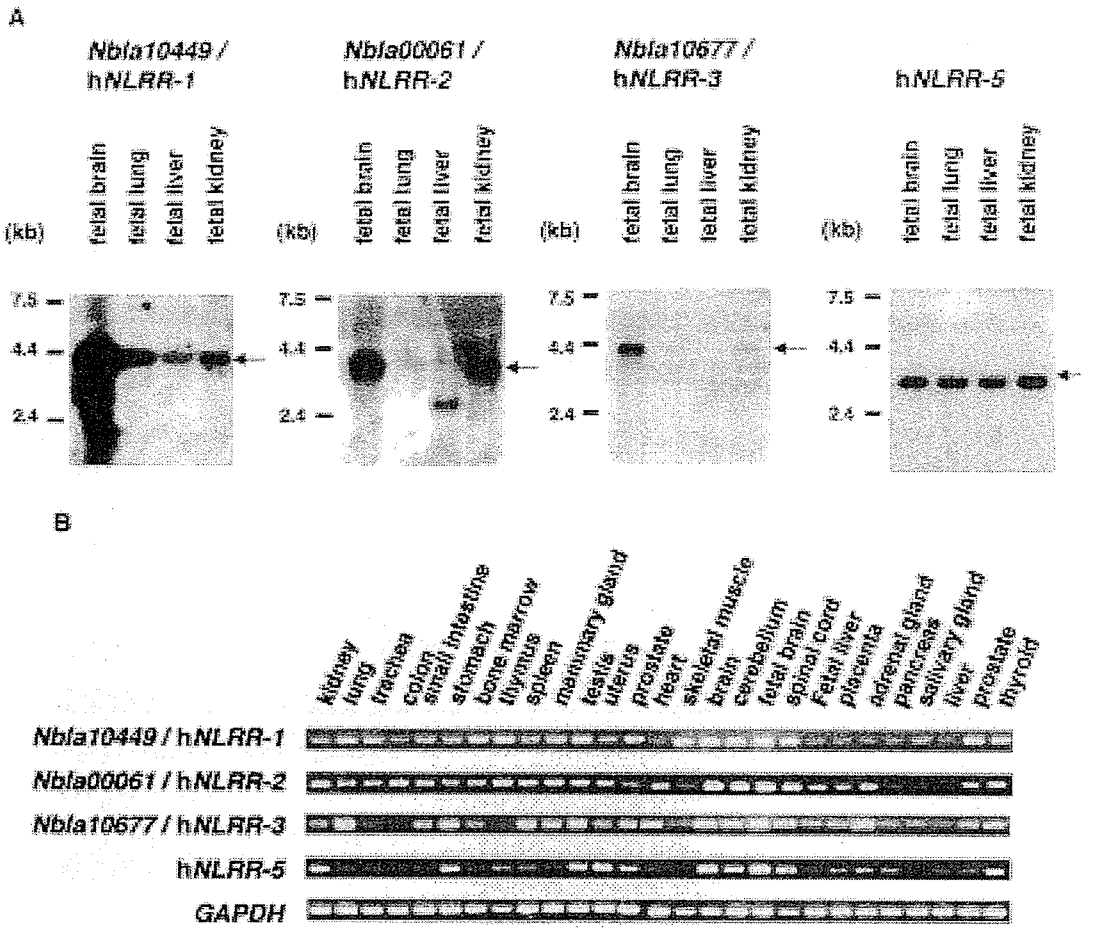

Figure 2. Expression of h*NLRR*s mRNA in human normal tissues. A, Northern blot analysis of h*NLRR*s mRNA in human fetal tissues. As a control for the amount of RNA, the same filter was rehybridized with ß-actin. B, Semi-quantitative RT-PCR of h*NLRR*s in multiple human tissues. Total RNA of 25 adult and 2 fetal tissues. As a control, same cDNA templates were amplified by *GAPDH* primers.

We then examined whether or not there was any genomic amplification of h*NLRR-1* or h*NLRR*-2 because that of *Nbla10449*/h*NLRR-1* was preferentially expressed in UF NBLs, and that of *GAC1*/h*NLRR-2* was reported to be amplified in the primary glioblastoma and anaplastic astrocytoma (15). However, our Southern blot analysis showed that neither of both genes was amplified in NBL cell lines so far examined (CHP134, IMR32, NB-9, NLF, TGW, NGP, NB69, NBL-S, SK-N-AS and SH-SY5Y) (data not shown). As regards the other cancer cell lines, expression of h*NLRR* family members was relatively restricted to the osteosarcoma and rhabdomyosarcoma cell lines (Fig. 3C). The low levels of h*NLRR*-3 and h*NLRR-5* expression were also seen in melanoma cell lines. Furthermore, expression of h*NLRR-2* was observed in the cell lines of colon, thyroid (medullary thyroid cancer), esophagus and lung. These results suggested that h*NLRR*s were preferentially expressed in the cell lines derived from neural crest cells.

Changes in expression of the NLRR family genes during NGF-induced differentiation and NGF-depletion-induced apoptosis in newborn mouse SCG neurons in primary culture. To investigate the role of NLRR family molecules in NGF/TrkA-mediated signaling, we next used newborn mouse SCG neurons, from which NBL is derived. As reported previously, NGF induced marked morphological differentiation of SCG neurons (14). NGF-induced neurite extension was observed on day 2 and was enhanced thereafter by increasing in number and length (Fig. 4A, NGF^+). The depletion of NGF by treating the cells with anti-NGF antibody induced neuronal programmed cell death (Fig. 4A, NGF^-). As shown in Fig. 4B, expression of m*NLRR-1* and m*NLRR-5* was down-regulated during NGF-induced neuronal differentiation, and was up-regulated after NGF deprivation (Fig. 4B). On the other hand, expression of m*NLRR-2* and m*NLRR-3* was slightly up-regulated when they were treated with NGF, and was significantly down-regulated after NGF deprivation (Fig. 4B), suggesting that expression of m*NLRR* genes might be related to the NGF signaling.

Prognostic significance of expression of Nbla10449/hNLRR-1 and Nbla10677/hNLRR-3 in primary neuroblastomas. To evaluate the clinical significance, expression of *Nbla10449/*h*NLRR-1* and *Nbla10677*/h*NLRR-3* in 99 NBLs was statistically analyzed. Table I gives the mean and standard error (SEM) of h*NLRR-1/Nbla10449* and h*NLRR-3/Nbla10677*

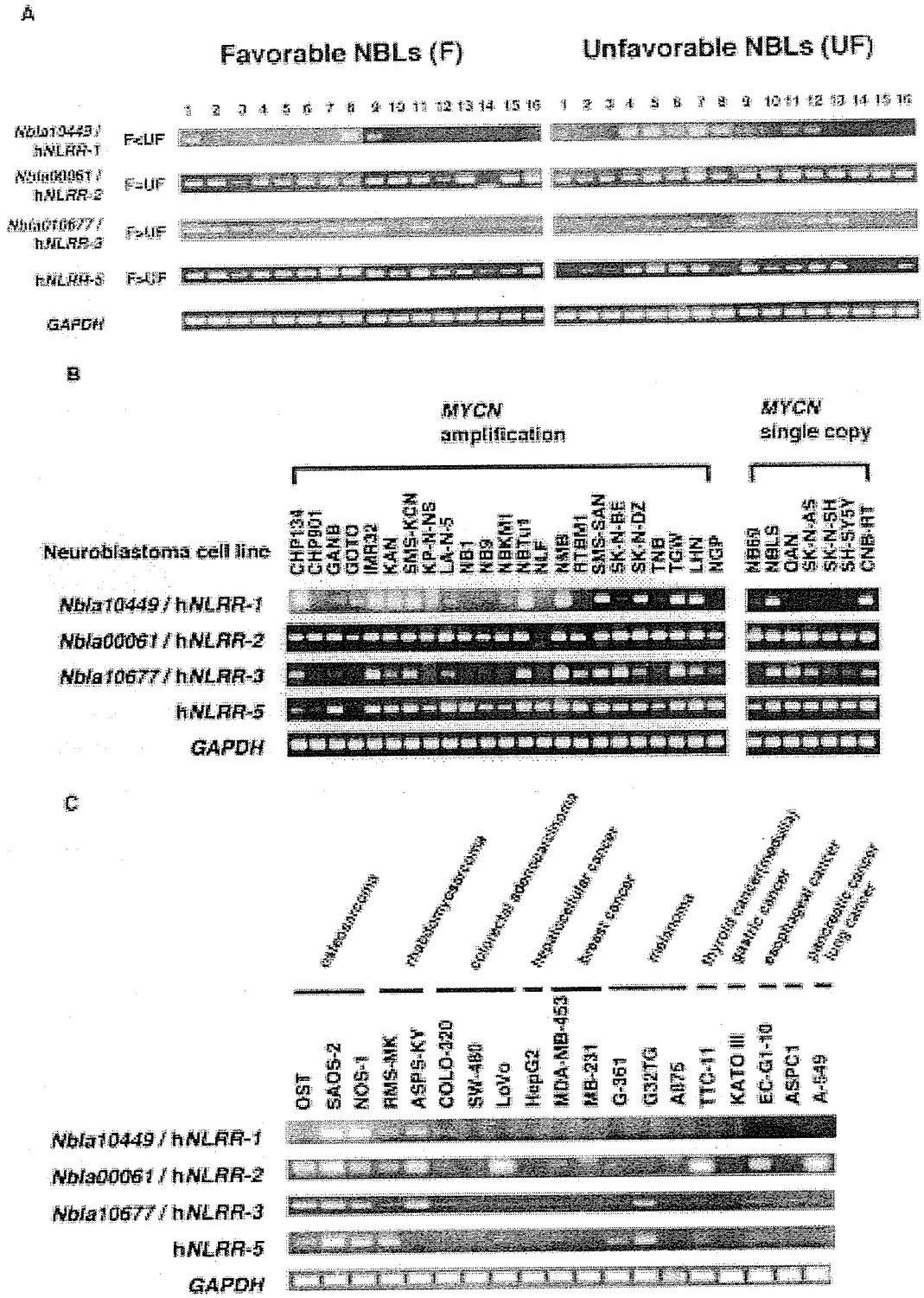

Figure 3. Expression of h*NLRR* family genes in primary NBLs, NBL cell lines and other cancer cell lines. A, Differential expression of h*NLRR* family genes in 16 favorable and 16 unfavorable NBLs. mRNA expression was detected by semi-quantitative RT-PCR procedure. The expression of *GAPDH* is shown as a control. Lanes 1-16: favorable NBLs (F, stage 1 or 2, with a single copy of *MYCN*), lanes 17-32: unfavorable NBLs (UF, stage 3 or 4, with *MYCN* amplification). B, Expression of h*NLRR*s mRNA in NBL cell lines. Twenty-three NBL cell lines with *MYCN* amplification and 7 cell lines with a single copy of *MYCN* were used for semi-quantitative RT-PCR as templates. C, Expression of h*NLRR*s mRNA in the other cancer cell lines. Semi-quantitative RT-PCR analysis was performed using cDNA and control *GAPDH* primers. Tumor origins are shown on the top.

expression by age, tumor stage, *TrkA* expression, *MYCN* copy number, origin, and mass screening. High expression of h*NLRR-1/Nbla10449* were significantly associated with >1 year of age (p=0.0001), advanced stage (p=0.0007), low expression of *TrkA* (p=0.011), *MYCN* amplification (p=0.0001) and sporadic tumors (p=0.0004), but not with the tumor origin (p=0.4). The results of log-rank test showed that a high level of h*NLRR-1/Nbla10449* expression was significantly associated

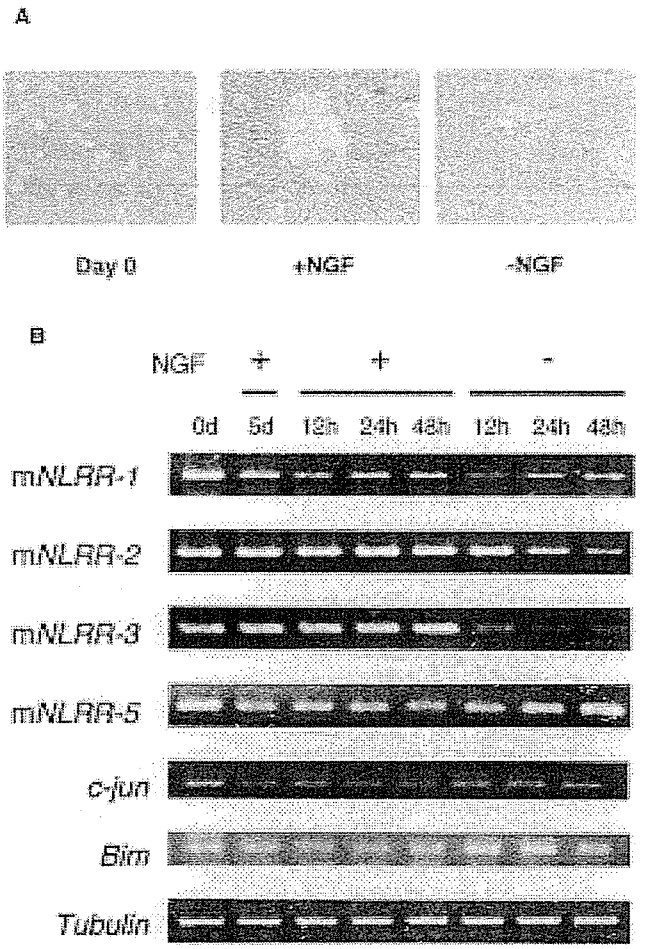

Figure 4. Changes in mRNA expression of mouse *NLRR* family genes in mouse superior cervical ganglion (SCG) cells treated with NGF in primary culture. A, Effect of NGF on newborn mouse SCG neurons in primary culture. The pictures were taken on day 0 and 5 (NGF^+) in the presence of 50 ng/ml NGF. NGF was then depleted from the medium by adding 1% v/v anti-NGF antibody for 36 h (NGF^-). B, Changes in expression of m*NLRR*s mRNA during NGF-induced differentiation and NGF depletion-induced apoptosis in newborn mouse SCG neurons in primary culture. SCG neurons were cultured for 5 days with NGF and then further cultured with or without NGF for 12, 24, 48 h. *c-jun* and *Bim*, positive control gene; Tubulin, used for standardization of the cDNA concentration.

with an unfavorable outcome (p=0.028). On the other hand, there was significant correlation between high levels of *Nbla10677*/h*NLRR-3* expression and younger age (p=0.0018), favorable stage (p=0.0007), high levels of *TrkA* expression (p=0.021), single copy of *MYCN* (p=0.0002) and the tumors found by mass screening (p=0.0049), but not with the tumor origin (p=0.33).

The univariate Cox regression was employed to examine the individual relationship of each variable to survival (Table II). These variables were: h*NLRR-1*/*Nbla10449* (log), h*NLRR-3*/*Nbla10677* (log), age (>1 year vs. <1 year), tumor stage (3+4 vs. 1+2+4s, *MYCN* copy number (1 copy vs. >1 copy), mass screening (+ vs. -), and origin (adrenal gland vs. others). Expression of h*NLRR-1*/*Nbla10449* (p=0.005), age (p<0.0005), *MYCN* copy number (p<0.0005), mass screening (p=0.001) were found to be statistically of prognostic importance. The results in Table II show that h*NLRR-1*/

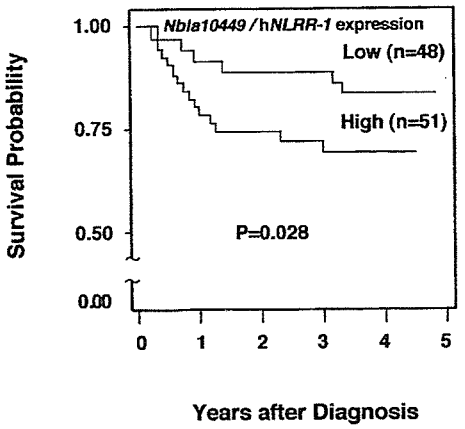

Figure 5. Kaplan-Meier survival curves for the 48 patients with low expression and the 51 patients with high expression.

Nbla10449 expression was an independent prognostic factor from age, *MYCN* copy number and mass screening in primary NBLs.

Discussion

In the present study, we identified the full-length human neuronal leucine-rich repeat protein (*NLRR*) family genes preferentially expressed in the nervous system and adrenal gland: *Nbla10449*/h*NLRR-1*, *Nbla00061*/h*NLRR-2*/*GAC1*, *Nbla10677*/h*NLRR-3* and h*NLRR-5*. In primary NBLs, the levels of h*NLRR-1* expression are significantly higher in the unfavorable subsets than those in the favorable tumors, whereas the expression pattern of h*NLRR-3* and h*NLRR-5* is the opposite. The results from the experiments using mouse SCG neurons treated with NGF in the primary culture have suggested that both m*NLRR-2* and *NLRR-3* are the molecules relating to promotion of neuronal survival or differentiation, while m*NLRR-1* and m*NLRR-5* function as those promoting cell growth or enhancing apoptosis. Furthermore, expression of h*NLRR-1* has been found as a significant indicator of poor outcome of NBLs, whereas that of h*NLRR-3* is associated with other favorable prognostic factors. Thus, hNLRR family members appear to differently regulate functions of neuronal cells as well as those of neuroblastoma.

A protein with leucine-rich repeat (LRR) domains was first identified in an α-2-glycoprotein of human serum (17). LRR-containing proteins represent a diverse group of molecules with different functions and cellular locations in a variety of organs. LRR domains provide an ideal conformation for binding to other proteins and this structure is thought to be involved in protein-protein interaction (10). Many LRR-containing proteins have been shown to function as cell-adhesion molecules or signaling receptors and are implicated in a variety of events in neural development. For example, adhesive LRR-containing proteins and small proteoglycans such as osteoinductive factor (OIF) bind various components of the extracellular matrix and growth factors. Interestingly, OIF binds the transforming growth factors, TGF-ß and TGF-ß2, and is involved in bone formation (18). The neurotrophin receptors, Trks, also possess the LRR domains in the extra-

Table I. Correlation between expression of *Nbla10449/hNLRR-1* or *Nbla10677/hNLRR-3* and other prognostic factors (Student's t-test).

Variable	No.	*Nbla10449/hNLRR-1* Mean ± SEM	*Nbla10449/hNLRR-1* p-value	*Nbla10677/hNLRR-3* Mean ± SEM	*Nbla10677/hNLRR-3* p-value
Age					
<1 year	63	0.84±0.21	0.0001	5.05±0.93	0.0018
>1 year	36	3.97±1.44		2.53±0.77	
Tumor stage					
1, 2, 4s	57	0.68±0.17	0.0007	5.36±1.00	0.0007
3, 4	42	3.74±1.25		2.48±0.68	
TrkA expression					
Low	45	3.50±1.17	0.011	3.13±0.77	0.021
High	54	0.71±0.18		4.97±1.02	
MYCN copy no.					
Amplified	29	5.19±1.75	0.0001	1.71±0.90	0.0002
Single	70	0.65±0.14		5.14±0.86	
Origin					
Adrenal gland	63	2.16±0.75	0.4	4.18±0.90	0.33
Others	36	1.67±0.79		4.06±0.93	
Mass screening					
+	54	0.67±0.18	0.0004	5.09±1.02	0.0049
-	45	3.55±1.17		2.98±0.76	

Table II. Cox regression models using *Nbla10449/hNLRR-1* expression and dichotomous factors of age, *TrkA* expression, *MYCN* amplification, and origin (n=99).

Model	Variable	p-value
A	*Nbla10449/hNLRR-1*	0.005
B	*Nbla10677/hNLRR-3*	0.15
C	Age (>1 vs. <1 year)	<0.005
D	*MYCN* (1 copy vs. amplification)	<0.005
E	Origin (adrenal gland vs. others)	0.079
F	Mass screening (+ vs. -)	0.001

cellular region. In *Drosophila*, some LRR domain-containing molecules such as toll, slit, connectin, chaoptin and tartan play an important role in regulating neural development (19-23).

The LRR motif includes highly hydrophobic amino acids and a repeat structure consisting of about 24 residues (20). NLRR family proteins contain in its extracellular region an immunoglobulin C-2 type domain and a fibronectin type III domain in addition to 11 sets of LRR motif (24). *NLRR* family genes were first isolated from a mouse brain cDNA library (16,25), and then 3 distinct isoforms (m*NLRR-1*, m*NLRR-2* and m*NLRR-3*) have been identified in zebrafish, *Xenopus*, mouse, rat and *Macaca facicularis* (16,24-26). The function of these NLRR proteins is poorly understood except that expression of m*NLRR-3* was increased after cortical brain injury (27) and that *rNLRR-3* expression is regulated through the Ras-MAPK signaling pathway in fibroblasts (28).

The deduced amino acid sequences of hNLRRs are highly conserved in the domains of LRR, LRRNT, LRRCT, Igc2 and FNIII, except that h*NLRR-5* does not have the FNIII domain. Many LRR proteins with LRRNT and LRRCT domains have been proposed to function in the regulation of neural differentiation and/or developmental processes as adhesive proteins and/or receptors (10). In addition to LRR, the Igc2 and FNIII domains in the extracellular region are often found in the molecules expressed in the central nervous system (26) and in several neuronal cell-adhesion molecules of the immunoglobulin superfamily such as N-CAM and L1 (29). Although hNLRRs and other NLRRs have no known signaling domain in the cytoplasmic region, a number of conserved stretches are found (Fig. 1). Especially, NLRR-1 and NLRR-3 have been shown to have a conserved stretch of 11 amino acids (ELYPPLINLWE) with 2 clathrin mediated endocytosis motifs, a tyrosine-based signal conforming to the YXRF motif (30,31), and a dileucine-type motif (32). Endocytosis and recycling mechanisms are relevant for cell adhesion molecules like integrins during cell migration (33,34).

Although the function of NLRR protein is poorly understood, there are some clues in recent reports. mNLRR-3 expression is increased in layers 2-3 in cerebral cortex after cortical injury, suggesting that this molecule plays a role in

the regulation of synaptic re-organization (27). zNLRR has also been proposed to have function as a neuronal-specific adhesion molecule or soluble ligand binding receptor during regeneration of the zebrafish central nervous system after injury, because retinal ganglion cells and descending spinal cord neurons strongly increased expression of *zNLRR* after axotomy in the adult (24).

The SCG/NGF system utilized in this study also provides a helpful hint to consider the neuronal function of hNLRRs. NLRR-1 may be involved in growth promotion in NBL by suppressing neuronal differentiation according to the result showing that the expression of m*NLRR-1* is down-regulated when the cells were treated with NGF. On the other hand, NLRR-3 may play a role in regulating differentiation to extend neurites and in neuronal survival of NBL cells since the expression of m*NLRR-3* was up-regulated by NGF and down-regulated after deprivation of NGF. These results are consistent with their differential expression pattern between favorable and unfavorable subsets of NBL.

In favorable NBLs as well as the cell lines with a single copy of *MYCN*, h*NLRR-1* expression was low as compared with the *MYCN*-amplified cells, suggesting that MYCN could influence the h*NLRR-1* expression. Interestingly, we have identified MYCN transcription factor-binding motifs (E-boxes) in the promoter region of the *NLRR-1* gene. Like h*NLRR-3*, h*NLRR-2* may also be involved in controlling neural cell survival as supposed from the result obtained in the NGF/SCG system. Ubiquitous h*NLRR-2* expression in NBLs suggests that h*NLRR-2* plays a role in maintaining cell survival. Of interest, h*NLRR-2* is often amplified in glioma as described below. h*NLRR-5* shows similar change in expression to h*NLRR-1* in the system of NGF-treated SCG neurons, albeit it is highly expressed in favorable NBLs. This suggests that hNLRR-5 may function as a proapoptotic molecule in NBL. Thus, each hNLRR member may have distinct biological function in NBL as well as neuronal cells. As the deduced intracellular region at the extreme C-terminus of hNLRR proteins has variable amino acid sequences, it may play a role in determining the differential function of hNLRR family receptors.

There are a few reports showing the relationship between LRR or NLRR and human cancer. *GAC1 (hNLRR-2)*, mapped to chromosome 1q32.1, is amplified and overexpressed in glioblastoma multiforme and anaplastic astrocytoma (15). Another report shows that expression of r*NLRR-3*, which was cloned by the subtractive screening using fibrosarcoma cells overexpressing c-Ha-ras, is regulated through the Ras-MAPK pathway, albeit the role in cancer cells is unknown (28). Trk family receptor tyrosine kinases have 3 LRRs in the extracellular domain, whose alteration can cause onco genic activation in some cancers (35). Interestingly, TrkA and TrkB also show an inverse expression pattern between favorable and unfavorable NBLs, that is very similar to the pattern of h*NLRR-1* and h*NLRR-3* expression. Since expression levels of TrkA and TrkB are powerful prognostic factors in NBLs, those of h*NLRR-1* and h*NLRR-3* may also be important in predicting the patient's outcome. Indeed, our present data suggest that expression of both hNLRR-1 and hNLRR-3 is inversely associated with the prognosis as well as other prognostic factors.

Acknowledgements

The authors thank Drs M. Fukumura, and H. Tsunobuchi for helpful discussions, Drs H. Kageyama and K. Miyazaki for experimental support, Dr S. Sakiyama for encouragement, and Ms. N. Sugimitsu and A. Morohashi for their excellent technical assistance. The authors also thank the following institutes for providing surgical samples: First Department of Surgery, Hokkaido University School of Medicine; Department of Pediatrics, National Sapporo Hospital; Department of Pediatric Surgery, Tohoku University School of Medicine; Department of Surgery, Gunma Children's Medical Center; Department of Pediatrics, Pediatric Surgery and General Surgery, Jichi Medical University; Department of Hematology and Oncology, Saitama Children's Medical Center; Department of Pediatrics, Juntendo University School of Medicine; Department of Surgery, Kiyose Metropolitan Children's Hospital; Department of Surgery and Pathology, Chiba Children's Hospital; Department of Pediatric Surgery, Chiba University School of Medicine; Department of Pediatric Surgery, Kimitsu Central Hospital; Department of Pediatric Surgery, Niigata University School of Medicine; Department of Pediatrics and Pediatric Surgery, Aichi Medical University; Department of Pediatrics, Kyoto Prefectural Medical University; Tumor Board, Hyogo Children's Hospital; Department of Pediatrics and Pediatric Surgery, Kagoshima University School of Medicine; Department of Pediatric Surgery, Showa University School of Medicine; Department of Pediatrics, Oita University School of Medicine; Department of Pediatric Surgery, Ohta General Hospital; Department of Pediatrics, Ichinomiya City Hospital; Department of Pediatric Surgery, Osaka City General Hospital; Department of Pediatrics, Nihon University School of Medicine Itabashi Hospital; Department of Pediatric Surgery, University of Tsukuba School of Medicine.

References

1. Bolande RP: The neurocristopathies. A unifying concept of disease arising in neural crest maldevelopement. Hum Pathol 5: 409-429, 1974.
2. Lo L, Morin X, Brunet JF and Anderson DJ: Specification of neurotransmitter identity by Phox2 proteins in neural crest stem cells. Neuron 22: 693-705, 1999.
3. Nakagawara A, Arima-Nakagawara M, Scavarda NJ, Azar CG, Cantor AB and Brodeur GM: Association between high levels of expression of the TRK gene and favorable outcome in human neuroblastoma. N Engl J Med 328: 847-854, 1993.
4. Nakagawara A, Azar CG, Scavarda NJ and Brodeur GM: Expression and function of TRK-B and BDNF in human neuroblastomas. Mol Cell Biol 14: 759-767, 1994.
5. Lasorella A, Noseda M, Beyna M, Yokota Y and Iavarone A: Id2 is a retinoblastoma protein target and mediates signaling by Myc oncoprotein. Nature 407: 592-598, 2000.
6. Ohira M, Shishikura T, Kawamoto T, Inuzuka H, Morohashi A, Takayasu H, Kageyama H, Takada N, Takahashi M, Sakiyama S, Suzuki Y, Sugano S, Kuma H, Nozawa I and Nakagawara A: Hunting the subset-specific genes of neuroblastoma: expression profiling and differential screening of the full-length-enriched oligo-capping cDNA libraries. Med Pediatr Oncol 35: 547-549, 2000.
7. Suzuki Y, Yoshitomo-Nakagawa K, Maruyama K, Suyama A and Sugano S: Construction and characterization of a full length-enriched and a 5'-end-enriched cDNA library. Gene 200: 149-156, 1997.

8. Ohira M, Morohashi A, Inuzuka H, Shishikura T, Kawamoto T, Kageyama T, Nakamura Y, Isogai E, Takayasu H, Sakiyama S, Suzuki Y, Sugano S, Goto T, Sato S and Nakagawara A: Expression profiling and characterization of 4200 genes cloned from primary neuroblastomas: identification of 305 genes differentially expressed between favorable and unfavorable subsets. Oncogene 22: 5525-5536, 2003.
9. Ohira M, Morohashi A, Nakamura Y, Isogai E, Furuya K, Hamano S, Machida T, Aoyama, Fukumura M, Miyazaki K, Suzuki Y, Sugano S, Hirato J and Nakagawara A: Neuroblastoma oligo-capping cDNA project: toward the understanding of the genesis and biology of neuroblastoma. Cancer Lett 197: 63-68, 2003.
10. Kobe B and Deisenhofer J: The leucine-rich repeat: a versatile binding motif. Trends Biochem Sci 19: 415-421, 1994.
11. Shimada H, Chatten J, Newton WA Jr, Sachs N, Hamoudi AB, Chiba T, Marsden HB and Misugi K: Histopathologic prognostic factors in neuroblastic tumors: definition of subtypes of ganglioneuroblastoma and an age-linked classification of neuroblastomas. J Natl Cancer Inst 73: 405-416, 1984.
12. Brodeur GM, Pritchard J, Berthold F, Carlsen NL, Castel V, Castelberry RP, De Bernardi B, Evans AE, Favrot M and Hedborg F: Revisions of the international criteria for neuroblastoma diagnosis, staging and response to treatment. J Clin Oncol 11: 1466-1477, 1993.
13. Kaneko M, Nishihira H, Mugishima H, Ohnuma N, Nakada K, Kawa K, Fukuzawa M, Suita S, Sera Y and Tsuchida Y: Stratification of treatment of stage 4 neuroblastoma patients based on N-myc amplification status. Study Group of Japan for Treatment of Advanced Neuroblastoma, Tokyo, Japan. Med Pediatr Oncol 31: 1-7, 1998.
14. Smith CJ, Johnson EM Jr, Osborne P, Freeman RS and Neveu I and Brachet P: NGF deprivation and neuronal degeneration trigger altered beta-amyloid precursor protein gene expression in the rat superior cervical ganglia *in vivo* and *in vitro*. Brain Res Mol Brain Res 17: 328-334, 1993.
15. Almeida A, Zhu XX, Vogt N, Tyagi R, Muleris M, Dutrillaux AM, Dutrillaux B, Ross D, Malfoy B and Hanash S: GAC1, a new member of the leucine-rich repeat superfamily on chromosome band 1q32.1, is amplified and overexpressed in malignant gliomas. Oncogene 16: 2997-3002, 1998.
16. Taguchi A, Wanaka A, Mori T, Matsumoto K, Imai Y, Tagaki T and Tohyama M: Molecular cloning of novel leucine-rich repeat proteins and their expression in the developing mouse nervous system. Brain Res Mol Brain Res 35: 31-40, 1996.
17. Takahashi N, Takahashi Y and Putnam FW: Periodicity of leucine and tandem repetition of a 24-amino acid segment in the primary structure of leucine-rich alpha 2-glycoprotein of human serum. Proc Natl Acad Sci USA 82: 1906-1910, 1985.
18. Kresse H, Hausser H and Schonherr E: Small proteoglycans. Experientia 49: 403-416, 1993.
19. Lemaitre B, Nicolas E, Michaut L, Reichhart JM and Hoffmann JA: The dorsoventral regulatory gene cassette spatzle/Toll/cactus controls the potent antifungal response in *Drosophila* adults. Cell 86: 973-983, 1996.
20. Rothberg JM, Jacobs JR, Goodman CS and Artavanis-Tsakonas S: Slit: an extracellular protein necessary for development of midline glia and commissural axon pathways contains both EGF and LRR domains. Genes Dev 4: 2169-2187, 1990.
21. Nose A, Mahajan VB and Goodman CS: Connectin: a homophilic cell adhesion molecule expressed on a subset of muscles and the motoneurons that innervate them in *Drosophila*. Cell 70: 553-567, 1992.
22. Krantz DE and Zipursky SL: *Drosophila chaoptin*, a member of the leucine-rich repeat family, is a photoreceptor cell-specific adhesion molecule. EMBO J 9: 1969-1977, 1990.
23. Chang Z, Price BD, Bockheim S, Boedigheimer MJ, Smith R and Laughon A: Molecular and genetic characterization of the *Drosophila tartan* gene. Dev Biol 160: 315-332, 1993.
24. Bormann P, Roth LW, Andel D, Ackermann M and Reinhard E: zfNLRR, a novel leucine-rich repeat protein is preferentially expressed during regeneration in zebrafish. Mol Cell Neurosci 13: 167-179, 1999.
25. Taniguchi H, Tohyama M and Takagi T: Cloning and expression of a novel gene for a protein with leucine-rich repeats in the developing mouse nervous system. Brain Res Mol Brain Res 36: 45-52, 1996.
26. Hayata T, Uochi T and Asashima M: Molecular cloning of XNLRR-1, a *Xenopus* homolog of mouse neuronal leucine-rich repeat protein expressed in the developing *Xenopus* nervous system. Gene 221: 159-166, 1998.
27. Ishii N, Wanaka A and Tohyama M: Increased expression of NLRR-3 mRNA after cortical brain injury in mouse. Brain Res Mol Brain Res 40: 148-152, 1996.
28. Fukamachi K, Matsuoka Y, Kitanaka C, Kuchino Y and Tsuda H: Rat neuronal leucine-rich repeat protein-3: cloning and regulation of the gene expression. Biochem Biophys Res Commun 287: 257-263, 2001.
29. Brummendorf T and Rathjen FG: Structure/function relationships of axon-associated adhesion receptors of the immunoglobulin superfamily. Curr Opin Neurobiol 6: 584-593, 1996.
30. Chen WJ, Goldstein JL and Brown MS: NPXY, a sequence often found in cytoplasmic tails, is required for coated pit-mediated internalization of the low density lipoprotein receptor. J Biol Chem 265: 3116-3123, 1990.
31. Collawn JF, Stangel M, Kuhn LA, Esekogwu V, Jing SQ, Trowbridge IS and Tainer JA: Transferrin receptor internalization sequence YXRF implicates a tight turn as the structural recognition motif for endocytosis. Cell 63: 1061-1072, 1990.
32. Kirchhausen T: Clathrin. Annu Rev Biochem 69: 699-727, 2000.
33. Lauffenburger DA and Horwitz AF: Cell migration: a physically integrated molecular process. Cell 84: 359-369, 1996.
34. Lawson MA and Maxfield FR: Ca(2+)- and calcineurin-dependent recycling of an integrin to the front of migrating neutrophils. Nature 377: 75-79, 1995.
35. Meakin SO and Shooter EM: The nerve growth factor family of receptors. Trends Neurosci 15: 323-231, 1992.